HTTPS://DOI.ORG/10.25923/CCVG ZE70

BEST PRACTICES FOR INCORPORATING UAS IMAGE COLLECTION INTO WETLAND MONITORING EFFORTS: A Guide for Entry Level Users

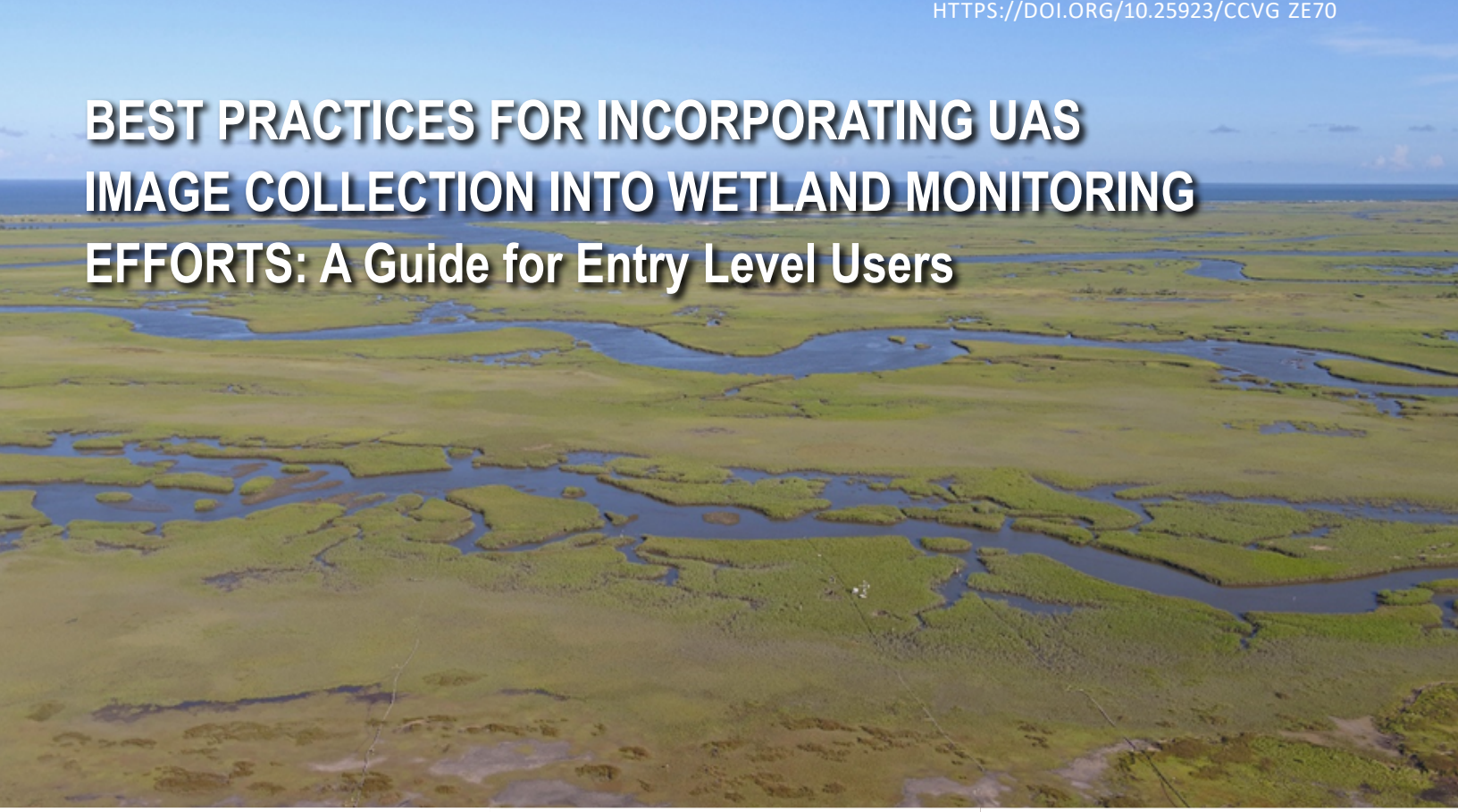

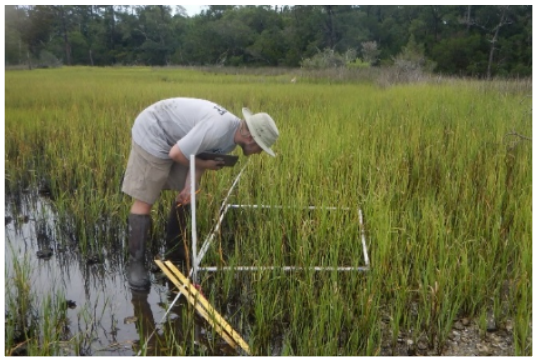

June 2022

NOAA TECHNICAL MEMORANDUM NOS NCCOS 308

NOAA NCCOS Marine Spatial Ecology Division

Citation
Davis, J., R. Giannelli, C. Falvo, B. Puckett, J. Ridge, and E. Smith. 2022. BEST PRACTICES FOR INCORPORATING UAS IMAGE COLLECTION INTO WETLAND MONITORING EFFORTS: A Guide for Entry Level Users. NOAA Technical Memorandum NOS NCCOS 308, Silver Spring, MD. 26 pps.

Cover photo credit: Erik Smith, North Inlet Winyah Bay NERR

.

https://doi.org/10.25923/ccvg-ze70

BEST PRACTICES FOR INCORPORATING UAS IMAGE COLLECTION INTO WETLAND MONITORING EFFORTS: A Guide for Entry Level Users

June, 2022

Authors:

Jenny Davis[1], Ryan Giannelli[2], Cristiana Falvo[3], Brandon Puckett[4]*, Justin Ridge[3], Erik Smith[5]

[1] NOAA National Ocean Service, National Centers for Coastal Ocean Science, Marine Spatial Ecology Division, Beaufort, NC
* current affiliation
[2] Consolidated Safety Services, Inc. under contract to NOAA
[3] Duke University Marine Laboratory, Division of Marine Science and Conservation, Nicholas School of the Environment, Duke University, Beaufort, North Carolina
[4] North Carolina National Estuarine Research Reserve, Beaufort NC
[5] North Inlet – Winyah Bay National Estuarine Research Reserve & University of South Carolina, Baruch Institute, Georgetown, SC

NOAA Technical Memorandum NOS NCCOS 308

United States Department of Commerce	National Oceanic and Atmospheric Administration	National Ocean Service
Gina M. Raimondo Secretary	Richard W. Spinrad Under Secretary	Nicole LeBoeuf Assistant Administrator

EXECUTIVE SUMMARY

Recent expansion in the availability of relatively inexpensive, uncrewed aircraft systems (UAS; aka "drones") has fueled widespread interest in their use in natural resource management. The high-resolution sensors that come standard with many UAS, combined with advancements in flight planning and image processing software enable the detection and quantification of change at spatial and temporal scales that are meaningful to natural resource managers. Despite the potential value of UAS for habitat monitoring programs, a lack of available guidance about how to best implement these technologies has been a barrier to their widespread adoption.

We describe a systematic effort to determine best practices for the use of UAS in wetland monitoring efforts. Specifics of flight planning, image collection, structure from motion processing, and habitat mapping are addressed. This guidance is tailored to entry level UAS users who aspire to use UAS to complement field monitoring efforts without becoming experts in image analysis. The results demonstrate that there is significant value to be gained through the incorporation of UAS into wetland monitoring. The guidance provided here is a collection of lessons learned that are provided with the goal of reducing the learning curve for new adopters of this technology.

KEY MESSAGES

1. It is possible to create high quality 2- and 3-dimensional data sets with a relatively inexpensive drone platform, basic RGB sensor, and minimal experience.
2. The use of Ground Control Points (GCPs) is necessary for minimizing vertical and horizontal model error. In cases where site conditions limit GCP placement density, ensuring they are evenly spaced is critical to achieving accurate imagery products.
3. UAS imagery-based bare earth models can achieve accuracies that are comparable to those of LiDAR derived models
4. UAS-collected imagery can be an effective predictor of live vegetative biomass. However, this was not found to be true for predicting vegetative percent cover and stem height.
5. Sensor to sensor variability necessitates cross-calibration when sensors are changed during the lifetime of a study.
6. Despite the current need for further method development and standardization, UAS are a valuable addition to wetland monitoring efforts.

Table of Contents

Commonly Used Acronyms

CHM – canopy height model

DEMs – digital elevation models

DSM – digital surface model

DTM – digital terrain model

GCP – ground control point

GSD – ground sampling distance

NCNERR – North Carolina National Estuarine Research Reserve

NDVI – normalized difference vegetation index

NERRS – National Estuarine Research Reserve System

NIR – near infrared

NIWB – North Inlet-Winyah Bay

RE – red edge

RGB – red green blue

RMSE – root mean square error

RTK-GNSS – real-time kinematic - global navigation satellite system

SfM – Structure-from-Motion

SLR – sea level rise

UAS – uncrewed aerial systems

1.0 INTRODUCTION

Vegetated intertidal wetlands are a dominant habitat type in coastal estuaries and are highly valued for the ecosystem services (e.g. habitat provision, water quality mediation) and protective benefits like shoreline stabilization and flood risk mitigation that they provide. Because coastal wetlands occupy the narrow zone between upland and open water regions, they are uniquely vulnerable to coastal storms and sea level rise and serve as sentinels of coastal change. Predictions of increasing rates of sea level rise (SLR) and concomitant increases in the frequency of coastal storms have fueled an interest in wetland monitoring for change detection. Changes in the relative elevation of a wetland within its local tidal frame for example, have important consequences for both the vulnerability of that wetland to future SLR and storms, and for the ecosystem services it provides. Monitoring programs designed to detect such change are critical for understanding wetland function, quantifying vulnerability to future stressors, and demonstrating the need for corrective action at highly vulnerable sites.

Technological advances that facilitate the cost-effective collection and processing of low-altitude imagery from uncrewed aerial systems (UAS's; aka "drones") have fueled an interest in incorporation of UAS-based approaches into wetland monitoring efforts. For the average wetland scientist who is not already well-versed in analysis of aerial imagery, adopting this technology may seem like a daunting proposition. A recent series of workshops among coastal researchers and managers in the southeastern U.S. identified the need for best practices and standardized approaches for the use of drones in coastal research as a barrier to their widespread use (Taylor et al, 2021). The goal of this contribution is to document our efforts at incorporating UAS imagery into ongoing wetland monitoring efforts as a first step toward addressing that need. We describe lessons learned and document best practices with respect to image collection, processing and interpretation with the goal of decreasing the learning curve for other investigators interested in using UAS for wetland monitoring.

1.1 Untapped Potential: The Case for UAS in Wetland Monitoring

Traditional approaches to wetland monitoring involve ground-based sampling efforts. Generally, these efforts include repeat measures of vegetative characteristics (community composition, total vegetative cover, canopy height, sediment surface elevation, etc.) at fixed sampling plots with the frequency of data collection dependent on the specific research questions being addressed (Peet et al., 1989, Roman et al., 2001). Sampling plot size typically ranges from 0.625 to 1 m^2. Plot level analyses are time and labor intensive; as a result, the total number of plots surveyed (often on the order of 20-30 per site) generally covers only a small fraction of the wetland in question. While plot level monitoring can yield highly accurate and repeatable data on vegetative structure at the scale of the individual plot, it can miss important spatial heterogeneity such as die-off patches, concentrated areas of wrack deposition and other events that may be important to understanding marsh function.

Historically, larger scale spatial detail in marshes has been addressed with the use of satellite imagery. Satellite imagery is often available for minimal charge and can be valuable for obtaining a bird's-eye view of the system in question. The most significant limitations to the use of satellite imagery for detecting change are that the user has no input into the timing of image collection and it can be challenging to find available repeat image sets that are consistent in their timing of collection with respect to season, cloud cover, and tidal stage, all of which can strongly influence or prevent interpretation. Further, satellite imagery often has insufficient resolution to detect change at spatial scales that are important to marsh managers.

UAS offer a low-cost (many off the shelf systems are available for < $1500), high-resolution option for limiting on-the-ground sampling while simultaneously increasing the extent of spatial coverage, resolution, and accuracy of monitoring results. Because UAS allow for the inexpensive collection of on-demand aerial images, they are invaluable for detecting changes on both long (e.g. response to sea level rise) and short (e.g. response to hurricanes) temporal scales. As such, UAS have the potential to radically improve traditional wetland monitoring efforts.

1.2 Challenges to Getting Started: "Activation Energy"

Previous investigators have predicted that ready access to commercial off the shelf UAS would "revolutionize" wetland science (Kalacska et al., 2017). To date, this prediction has not been realized, primarily due to a lack of readily available

guidance on optimal image collection techniques and post-processing of UAS-collected data (Assmann et al., 2018). Published research using UAS rarely documents the methodology, workflow, and practical information in sufficient enough detail to facilitate reproducibility and troubleshooting, especially for users with little experience in image collection and analysis (James et al., 2017, Joyce et al., 2018).

While it is possible for a novice user to collect imagery that is valuable for visual analysis of large-scale patterns and trends, products that lead to quantifiable and reproducible results (e.g. digital terrain models, estimates of vegetative cover and biomass, and delineation of ecotones and shorelines) require a level of image processing knowledge to create. For the entry-level user, developing a working understanding of how to optimize image capture and processing routines to create these products can be daunting and presents an obstacle to the wide-spread adoption of UAS as a standard tool in wetland monitoring programs.

Formally, "activation energy" is the minimum amount of energy required for a chemical reaction to take place. Colloquially, activation energy refers to the amount of effort one must exert to complete a given task. Our goal with this report is to decrease the activation energy required for a novice user to utilize UAS for wetland monitoring purposes.

1.3 Scope of This Document

This report describes the successes and failures associated with attempts to replicate ground-based monitoring results from UAS-collected aerial imagery. The work described here involved a systematic analysis of the impacts of image collection variables (e.g. sensors, ground sampling distance, seasonality) on the accuracy of image-based products. The UAS flight platforms used in this effort were all inexpensive, commercially available quadcopters as are commonly employed by entry level users or those with limited budgets. The sensors used include the optical (Red, Green, Blue; RGB) sensors that are standard with each platform as well as add-on multi-spectral sensors capable of capturing Near Infrared (NIR) and Red Edge (RE) bands.

The intended user will have familiarity with basic flight operations, regulations, and UAS licensing requirements in addition to experience with ArcGIS. This contribution does not review or make recommendations regarding UAS platform, sensor or software selection; several previous contributions have covered these topics (Dobroski 2019, Jeziorska, 2019). *This is not intended to be a comprehensive guidebook for UAS-based wetland monitoring. Our intention is to arm the novice user with the in-depth details that will provide the knowledge and confidence needed to generate reproducible and comparable results from UAS-acquired imagery.*

2.0 SUPPORTING RESEARCH

The data collection efforts that supported development of this guidance were conducted at three distinct sites. The first, Swan Island, Maryland, is part of the Smith Island complex in Chesapeake Bay. Swan Island is an uninhabited 25-acre island that was amended with dredged sediments in spring 2019, in an effort to enhance habitat diversity and bolster the resilience of this previously low-lying marsh island to sea level rise. Prior to sediment placement the island footprint was dominated by highly fragmented *Spartina alterniflora* marsh; after sediment placement and grading it was planted with *Spartina patens* and *S. alterniflora* at the appropriate elevations. The ultimate goal was establishment of a typical Mid-Atlantic salt marsh. Imagery collected at this site was evaluated for the sole purpose of investigating the role of ground control points (GCP's) in model accuracy. Results of this analysis guided GCP placement at the remaining sites. The other two sites are both part of the National Estuarine Research Reserve System (NERRS); a collection of 30 sites nationwide where NOS and states partner to promote research, education, and preservation of estuarine ecosystems. The North Inlet-Winyah Bay (NIWB) reserve is in Georgetown, South Carolina; the Masonboro Island site, near Wilmington, North Carolina, is part of the North Carolina NERR (NCNERR). Both sites are dominated by *S. alterniflora* at low elevations and transition to *S. patens, Distichlis spicata* and *Juncus romerianus* at higher elevations. Both NERR sites have ongoing ground-based wetland monitoring efforts in place, and thus were ideal for investigating the efficacy of incorporating UAS-based approaches into monitoring efforts.

At Swan Island, UAS flights were conducted in August 2019 with a DJI Phantom 4 Pro equipped with a 20 MP camera with 1-inch Complementary Metal Oxide Semiconductor (CMOS) sensor. Images were collected from an altitude of 40 m with a neutral density polarizing filter (ND8-PL) to minimize glare. A repeat set of flights was conducted using the same platform and flight plan in August 2021, this time with an additional sensor (Micasense RedEdge-MX ®) mounted to the airframe to collect multispectral images on the same flights that the built-in optical sensor collected RGB images.

At both of the NERRS sites, UAS flights were conducted in September of 2020 and February of 2021 to coincide with the timing of peak standing biomass (September) and minimum winter biomass (February). During both sampling periods, the area of interest was flown three times consecutively at three different altitudes (25 m, 50 m, 120 m) to determine the influence of ground sampling distance (GSD) on image-based product accuracy. At NIWB NERR, all flights were conducted with a DJI Matrice 200 V2 quadcopter equipped with a Micasense Altum sensor that simultaneously collects , R, G, B, NIR, RE, and thermal bands. At NCNERR, flights were conducted with a DJI Mavic 2 Pro quadcopter with a built-in Hasselblad sensor that was used to collect optical (RGB) imagery. Multispectral bands were collected simultaneously by a Sentera Double 4K that collects RGB, NIR and RE bands. To facilitate a direct comparison of the role of the sensor on UAS-based mapping products, an additional set of test flights were conducted at NCNERR in May of 2021. For these flights, both UAS-sensor combinations were flown in succession at an altitude of 50m.

All flights were conducted in a lawnmower pattern (parallel back and forth flight lines) using mission planning software to ensure constant altitude and image overlap (75% frontlap, and 75% sidelap) with a nadir camera angle. The same flight path was used for all repeat flights to ensure that the same area was covered across altitudes and seasons. UAS imagery were stitched together using commercially-available Structure-from-Motion (SfM) software Agisoft Metashape (v.1.6.1) and Pix4DMapper (v. 4.6.4) to generate continuous surface models of each site. All image data sets were processed using both software packages. Imagery was geolocated using GPS onboard the UAS platform, which attaches geotag information to each image during image collected, and georectified by incorporating Ground Control Point (GCP; described in section 3.2) data in the SfM software processing workflows.

All imagery data sets were processed according to the general workflow presented below (Figure 1). The SfM-derived products included orthomosaics (georectified composite images), Digital Surface Models (DSMs; for our purpose DSMs represent the image surface/canopy surface in regions where vegetation is present) and Digital Terrain Models (DTMs; 3D models in which the point cloud was filtered to remove all points that do not represent the ground surface). The DTMs created here are equivalent to lidar-generated “bare earth” models. SfM-generated products were imported into ArcGIS Pro 2.9 for calculation of total standing biomass, percent vegetative cover, and canopy height. Habitat maps (classified by vegetation type) were created in ArcGIS using the Classification Wizard. The following sections describe the lessons learned from these exercises and provide guidance on the optimal use of UAS for wetland monitoring.

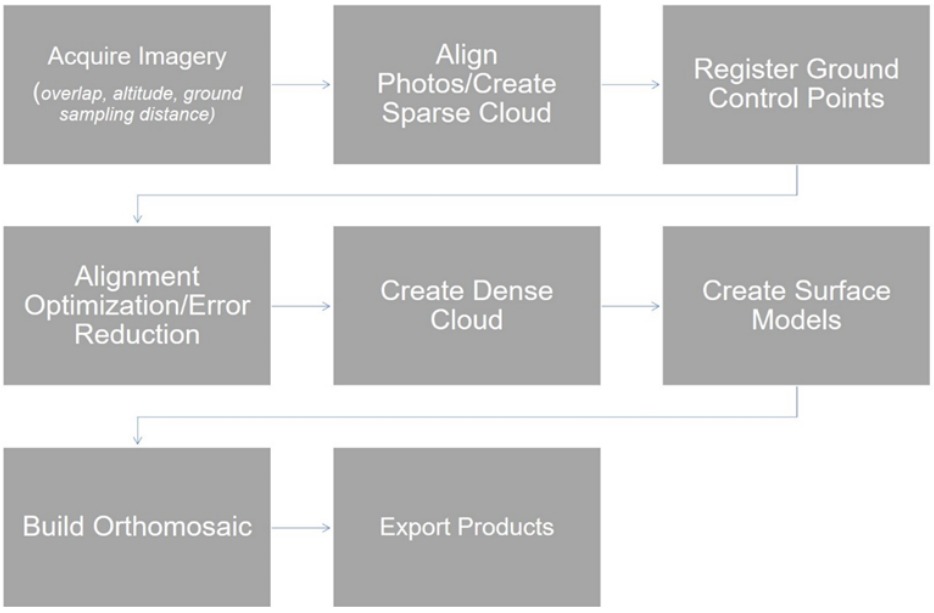

Figure 1. Imagery processing workflow.

3.0 IMAGE CAPTURE AND STRUCTURE FROM MOTION PROCESSING

3.1 Image Capture and Processing

3.1.1 Flight Planning

Image quality (and consequently, the quality of imagery-based products) is impacted by flight altitude, camera settings (shutter speed, focus, etc.), flight speed, and image overlap, among other factors. There are a range of mission planning/autopilot software products available, many of which interface seamlessly with the more common commercially available UAS platforms. **The use of mission planning software is critical to collecting high quality mapping data with ease.** All software packages used here (Drone Deploy, PiX4D Capture, and DJI Pilot) facilitated the collection of SfM-ready image data sets with minimal user input.

Standard flight pattern options include lawnmower (back and forth rows) and crosshatching (back and forth rows across the entire area once, and again 90o to the first grid). Flight patterns that involve crosshatching will necessarily result in longer flight times and large image sets. Crosshatching has been demonstrated to improve model resolution in systems with a high degree of topographic complexity (sparse forests, cityscapes, etc.; Swayze et al., 2021). **In tidal marshes, which tend to be homogenous in terms of topographic variability, serpentine flight patterns represent an optimal compromise among data density, and field time/battery requirements.** It is important that the flight boundaries extend beyond the area of interest (at least one flight line) for proper photogrammetric reconstruction of the entire area of interest.

3.1.2 Image Overlap

With SfM image processing, 3D marsh structure is computed from 2D imagery. SfM software aligns overlapping imagery acquired from multiple viewpoints based on matching identifiable features (i.e., tie points) within each image. Once the images are aligned, the SfM algorithm calculates the relative camera location from which each image was collected and based on the relative camera locations and overlap among images, computes the relative 3D locations of points in the 2D imagery by triangulation. The final step includes an optimization of the 3D structure through a bundle adjustment (a mathematical solution that minimizes the error between measured and modeled locations within the composite image; Westoby et al., 2012). The outputs of this process include a 3D point cloud where each point has corresponding positional data (x, y and z), a gridded DSM (where each cell in the grid represents a single elevation) and an orthorectified composite image.

Proper image alignment requires a minimum of 66% overlap among images. Greater overlap is recommended when the area of interest is relatively uniform and contains few distinct features with which to align imagery (Tmušić et al., 2020). Greater image overlap results in more common points between images, leading to less likelihood of having gaps in the composite image due to poor alignment, but comes at the expense of longer flight and post-processing times. **In this study, 75% frontlap and sidelap was found to consistently result in high resolution products. When collecting data simultaneously from two independent sensors on the same UAS, the mission should be planned around the sensor with the greater focal length. This ensures the minimum image overlap requirements will be met for both sensors.**

3.1.3 Additional Considerations for Image Collection

Adequate lighting is important for optimal photogrammetry products. The ability of SfM software to identify matching features is limited in areas of the imagery that are over-exposed or subject to dark shadows. The manufacturers of both multispectral sensors used here (Micasense and Sentera) recommend flying as close to solar noon as possible to eliminate shadows caused by low sun angles. Shadows within the imagery will alter the brightness values of specific pixels which can affect additional product generation such as habitat classification maps (Saha et al., 2005). Conversely, glare from areas of standing water (or wet soils) can result in oversaturation and lead to poor image alignment and decreased product accuracy (Saha et al., 2005). **For RGB sensors, the use of a circular polarizing filter (CPL) can help to eliminate unwanted light reflected when flying in high light conditions over wet surfaces.** Flight paths that involve flying into and away from the sun (rather than crossways) have been shown to further reduce glare (Slocum et al., 2019). Some mission planning software (e.g. Universal Ground Control Station) allow the user to set the orientation so that the drone always faces away from the sun, which may also help to reduce glare.

Flight altitude is an important controller of image quality (and therefore product quality). For a given sensor, lower flight altitude results in a smaller ground sampling distance (GSD; the amount of the land surface represented by a single pixel) a denser point cloud, and consequently, increased ability to resolve small features. However, lower flight altitude also results

in longer flight times (and more battery usage), a larger number of images collected, and the need for increased processing time/computing power and storage. In cases where the area of interest doesn't have many identifiable features (water, sandy beach, homogenous vegetative cover) a lower flight altitude may also lead to challenges with image alignment and therefore to lower accuracy products (Zimmerman et al., 2020). **In the tidal wetlands that we monitored, 50 m flight altitudes represented a reasonable tradeoff between resolution and flight time, and consistently resulted in images with enough unique characteristics to support image alignment.**

Consistent timing of flights is particularly important for the collection of multispectral imagery. Some multispectral sensors come with their own radiometric calibration reflectance panel which, when calibrated properly, will provide a reliable measurement of irradiance on the ground. We note that SfM software vary in their capacity to utilize information from reference panels to correct for differences in irradiance that occur during the course of image collection. At this time, Pix4D allows for the use of one set of reference images, Metashape allows for two (pre- and post- flight). Drone2map, another widely used software (though not used in the current effort) does not currently allow for any. This functionality is likely to change rapidly in response to advances in sensor technology. **It is advised to use pre- and post- flight calibration panels when possible as this helps to ensure consistency of results and therefore to facilitate comparison of data collected at different timepoints. In cases where the use of two sets of calibration panels is not possible, choose the set of calibration images taken in lighting that most closely mirrors the average lighting conditions for the entire flight.**

Wind can present an additional challenge for photogrammetric reconstruction of vegetated surfaces. Each UAS platform comes with a manufacturer-recommended wind threshold above which flights should not be attempted. Winds below this threshold may still present challenges including elevated battery usage which increases quadratically with wind speed, and deviations from the programmed course, which are particularly likely when the winds are gusty rather than constant. Many sensors are mounted on a gimbal which allows them to maintain a nadir position despite wind-induced pitch or roll of the airframe. When sensors are not gimbal-mounted, deviations of the airframe from vertical orientation will result in images being collected in different planes and consequently, changes in image overlap and sharpness. Winds that are strong enough to move the vegetation can pose an additional challenge to the production of accurate surface models as a given point in the canopy will not be in the same location in overlapping frames. **It is advisable to limit image collection efforts to periods of very light (< 10 kt) to no wind.**

If a DTM is among the desired imagery-based products, it will be important to fly at low tide when the marsh surface is exposed. **Ultimately, the choice of when to fly for optimal results requires balancing the influence of shadows, glare, wind, and tides; the ideal timing will vary among project sites and desired products.**

3.1.4 Structure from Motion Software

There are a large number of commercially available SfM software options to choose from. Previous comparisons have identified differences in the products generated by different softwares (Sona 2014, Pell et al., 2022). Our goal was to compare output products from two of the more widely used softwares (Metashape and Pix4D) for the purpose of understanding whether the products are directly interchangeable. We accomplished this by processing all 6 image sets from each NERRS twice; once in Metashape, and once in PiX4D, and comparing the output products. We followed the standard workflows provided by each SfM software producer with the specific settings detailed below:

Pix4DMapper. Key points were extracted at the full imagery resolution and image matching was set up for an aerial grid or pre-planned flight path. The number of key points was automatically determined and the calibration method was set to standard. A minimum of five images per band were identified by partial-automation to register each GCP in the software.

Agisoft Metashape. In Metashape, the software aligns imported images, approximating camera position and orientation to generate key points in the form of a sparse point cloud. A high accuracy was chosen for the photo alignment such that tie points were extracted from the full-resolution images. After alignment, GCPs were manually picked in order to georeference all images. Multiple steps of point filtering (step 4 in figure 1) were performed to eliminate erroneous points (i.e. points with high reconstruction uncertainty, projection accuracy, and reprojection error) within the sparse cloud. Camera and point optimization was performed after each round of point filtering according to the workflow documented by Over et al. (2021).

Consistency of modeled products was evaluated by comparisons of the positional accuracy of checkpoints and ground truth points (described below; section 3.2) in surface models generated by each software. **Comparison of the spatial accuracy of orthomosaics and DSMs generated by PiX4D and Metashape indicates that the products generated from both softwares are largely interchangeable. However, it is important to note that the default resolution of products differs by software;**

Metashape generates DSMs and DEMs (equivalent to PiX4D DTMs) at 2x the resolution of the orthomosaic while Pix4D generates DSMs at 1x GSD and DTMs at 5x GSD.

3.2 Influence of Ground Control on Model Accuracy

The creation of high accuracy maps without an RTK-GNSS equipped drone requires a mechanism for precision georeferencing of the collected imagery. This is typically accomplished with the use of visual reference markers or GCPs placed on the marsh surface within the footprint of the image collection area (Figure 2). Positional data (x, y, and z) collected from each marker with survey grade RTK-GNSS is used by the SfM software to reduce distortion of imagery-based products and translate products into a real-world coordinate system.

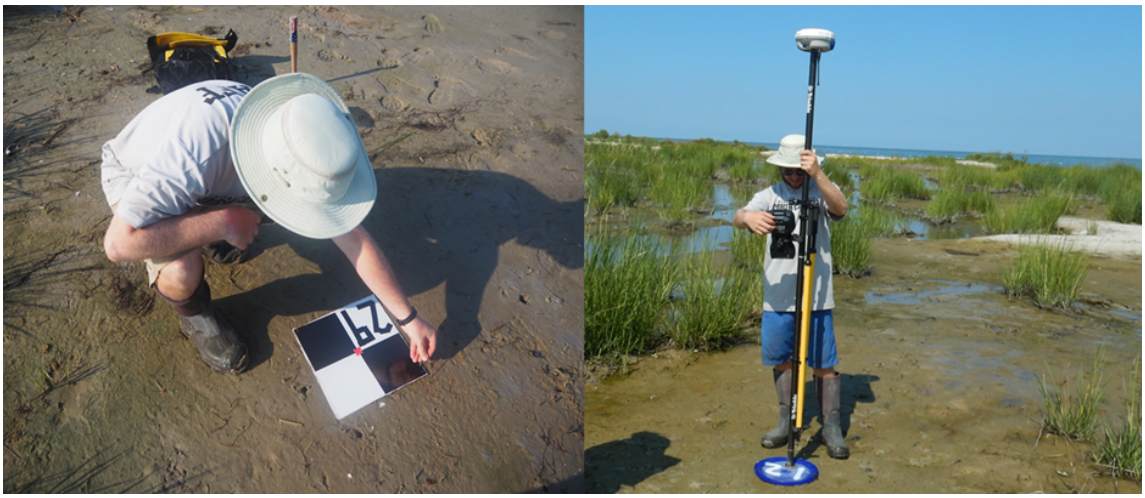

Figure 2. Ground control points (GCPs) can be any object that is easily visible from the air. Examples include black and white vinyl flooring tiles (left) and 5-gallon bucket lids (right). For optimal results, the precise location of GCP's should be established with survey grade GNSS. Photo Credit: NOAA/NCCOS

The influence of GCP density and placement on the accuracy of 3D reconstructions was investigated through the creation of a series of 3D models using the same set of imagery but with varying numbers of GCP's used in the SfM processing. The imagery used for this exercise was collected at Swan Island which was largely devoid of vegetation at the time of image collection. Due to the lack of vegetation, the SfM-generated bare earth surface models for Swan Island were more likely to represent the true ground surface than at vegetated sites where the presence of plants obscures the ground surface. As a result, this site allowed for a focused evaluation of the role of GCP placement in surface model accuracy. Twenty-four GCPs were placed during image collection. Model iterations involved the use of 3, 6, 12 and 24 GCPs which were equivalent to placement densities of 0.2, 0.5, 1, and 2 GCPs per hectare, respectively. The 3, 6, and 12 GCP model versions were each run twice; first selecting GCP's to ensure that they were evenly distributed across the modeled area, and a second time, selecting GCP's in such a way that they were clustered together and represented a limited portion of the entire site (Figure 3).

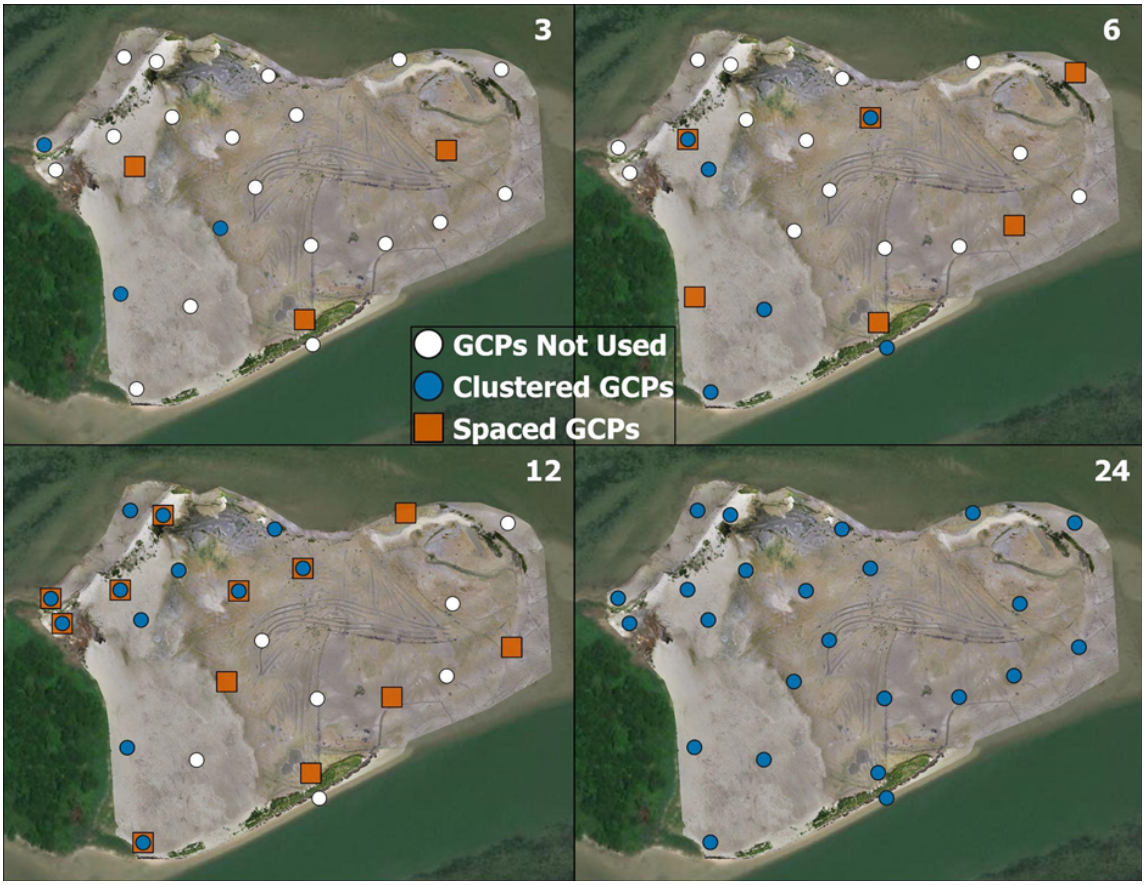

Figure 3. Ground control point analysis at Swan Island. Specific GCPs used in each iteration are indicated by colored symbols in the figure above. The number in the upper right corner of each image indicates total number of GCPs used to georeference each model. In the 3, 6, and 12 GCP iterations, all remaining GCP's that were not used to reference a given model iteration were used to calculate checkpoint error.

There are two metrics of model accuracy available in the standard reports generated by Pix4D and Metashape: Projection Error and Checkpoint Error. It is important to understand the difference between the two.

Projection error is the root mean square error among the measured (RTK-GNSS) and modeled (SfM-computed) positions of the GCPs that were used in model creation. The SfM process is designed to minimize projection errors by creating the best possible fit between modeled and measured GCP locations; as a result, projection errors are expected to be low. Comparison of projection errors among the Swan Island model iterations shows that error increases with increasing number and more even spacing of GCPs due to the challenge of fitting a model accurately to a large number of reference points (Figures 4 and 5). This trend underscores an important point: low projection error does not necessarily mean a better model, it can be the result of low GCP density or less than ideal placement.

Checkpoint error also involves comparison of modeled and measured GCP locations in terms of root mean square error, *but only for GCPs that were not used in the model construction process* (both PiX4D and Metashape provide the option to identify checkpoints). As a result, checkpoint error provides an independent measure of model accuracy that reflects the true differences between modeled and measured positions in image-based products. In the iterative GCP analysis described above, checkpoint error decreased as the number of GCPs used increased. The X and Y error of checkpoints was substantially larger in the model iteration involving 3 clustered GCPs (Figure 4). Vertical (Z) accuracy was negatively impacted by low GCP density and uneven placement and Z error was an order of magnitude greater than X/Y error with inadequate GCP placement (fewer than 12 evenly spaced GCPs; placement density of 1 GCP/hectare; Figure 4). This underscores another important point: GCPs are particularly important for increasing vertical accuracy. However, if the intended imagery-based products are limited to 2D maps, it is possible to obtain sub-decimeter accuracy with relatively sparse GCP placement. More importantly, comparison of projection and checkpoint accuracy shows that **the use of checkpoints in addition to GCPs is vital for understanding the fidelity with which SfM-modeled positions represent true positions on the ground.**

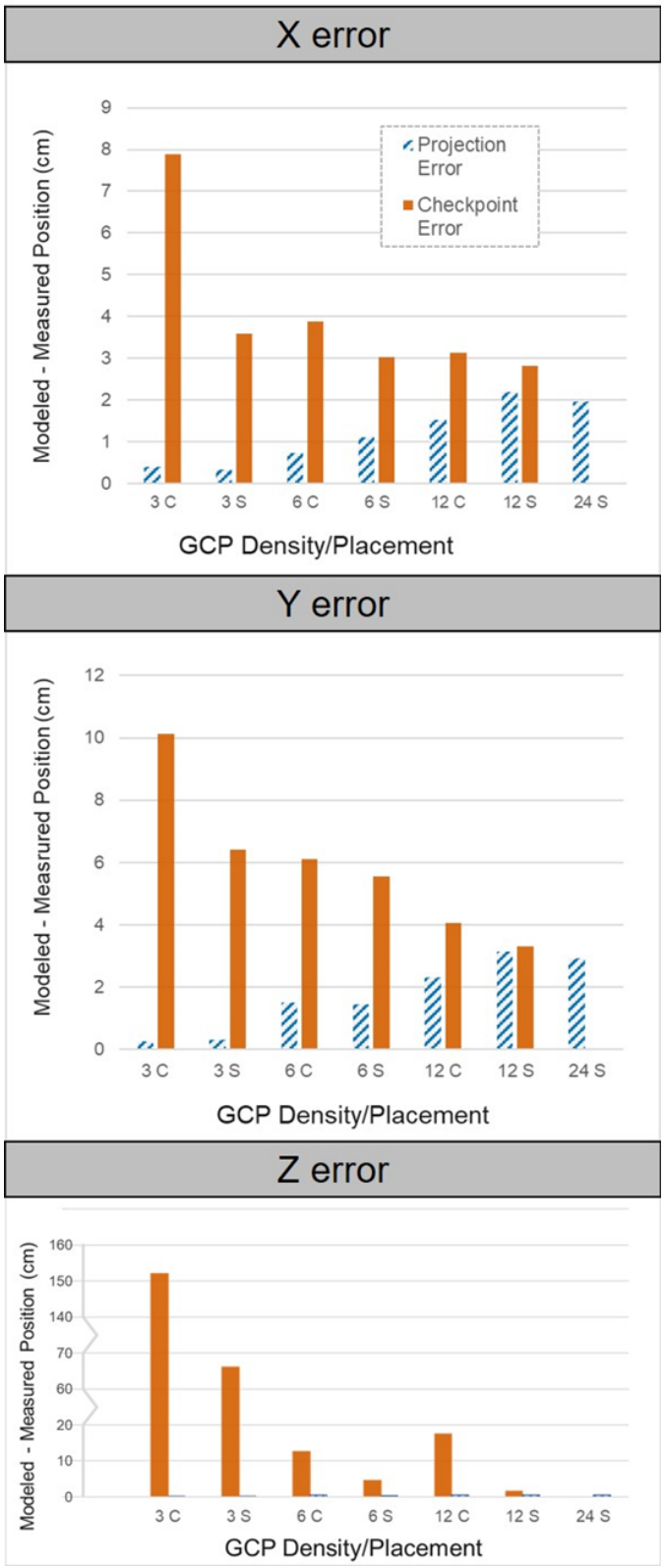

Figure 4. Positional Error of Structure from Motion (SfM)=generated projects as reported through the difference in modeled vs measured positions of ground control points (GCPs) that were used to generate the model (projection error) and GCPs that were not used to inform model construction (checkpoint error). Clustered GCP placement = C, Spaced = S.

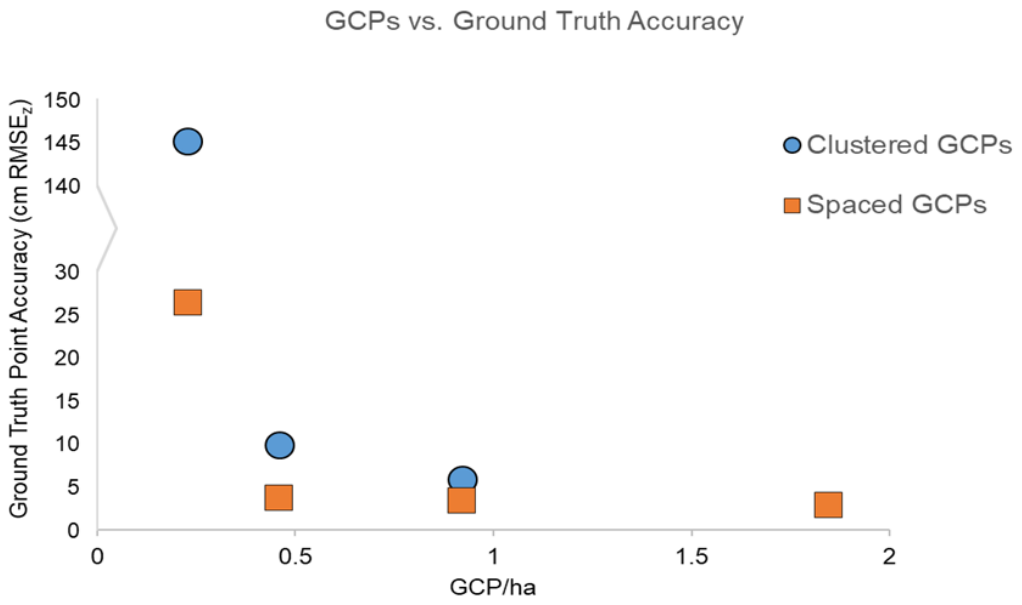

Figure 5. Vertical root mean square error (RMSEz) of ground truth points (n=80) as a function of the number of and distribution of GCP's used in SfM-based model construction. Note that 1 GCP/hectare is equivalent to 12 spaced GCP iteration in figure 4.

Ground truth points provide a further check on model accuracy. We define ground truth points as any additional locations in the modeled area for which position has been determined with high accuracy (i.e. RTK-GNSS). At Swan Island, ground truth data was collected at 80 fixed monitoring plots which were established as part of a long-term monitoring program for this site. Unlike the GCP-based checkpoints, these plots were not marked with visible markers. As a result, their locations are not visually identifiable in image products and it is not possible to evaluate their horizontal accuracy. Vertical accuracy of ground truth points was computed as the root mean square error between modeled and measured elevations at each of the 80 points. Vertical root mean square error (RMSEz) was calculated by loading the SfM-generated elevation models into ArcPro and using the Extract Values to Points tool to determine SfM-computed elevation at each of the ground truth point coordinates. As with the check point analysis, the vertical error of modeled elevations at ground truth points was dramatically reduced with greater density and more even distribution of GCPs (Figure 5).

This analysis involved imagery collected in 2019 when Swan Island had just recently been restored with dredged sediments and there was little vegetation present. As a result, the SfM-generated DSM represents bare earth conditions at this site. Overall, model accuracy was positively correlated with the number of GCP's used. The greatest accuracy was achieved when all 24 GCP's were included (equivalent to a density of 2 GCPs/hectare). This finding is consistent with previously published data from a similar analysis (Haskins et al., 2021). **While achieving 2 GCPs/ha is recommended where possible, the accuracy gained by increasing GCP density from 0.5 to 2.0 per hectare wasn't substantial as long as the GCP's were well-spaced. Further, depending on the size of the area in question and site conditions, this density is not always possible (e.g. marshes with unconsolidated sediments can be challenging to traverse on foot). When lower GCP density is necessary, optimal placement can go a long way toward optimizing 3D model accuracy (Santana et al., 2021). In addition, it is advisable to place extra GCPs as checkpoints, and/or to collect ground truth data as a metric of a model's positional accuracy.**

3.3 Model Validation

At sites with little vegetation, as in the Swan Island example above, SfM-generated surface models represent bare earth conditions; when vegetation is present they represent the approximate surface of the vegetative canopy. As a result, ground elevations are much more accurately represented in portions of a model where vegetation is sparse or non-existent. Additional processing (described below, section 3.4) can be applied to filter the point cloud to remove points that represent the vegetative canopy (or any other non-ground points). This process results in the production of a bare earth model referred to here as a DTM. Validation of this model requires the collection of ground truth data from areas with and without standing vegetation. In our experience, the degree to which vegetation can be fully filtered out, rendering a high accuracy DTM, is dependent on plant density and morphology which can vary widely across the spatial extent of an individual marsh (Figure 6). As a result, **it is important to collect validation (aka ground truth data) that represents the diversity of habitats and vegetation types in the area of interest** (Figure 6).

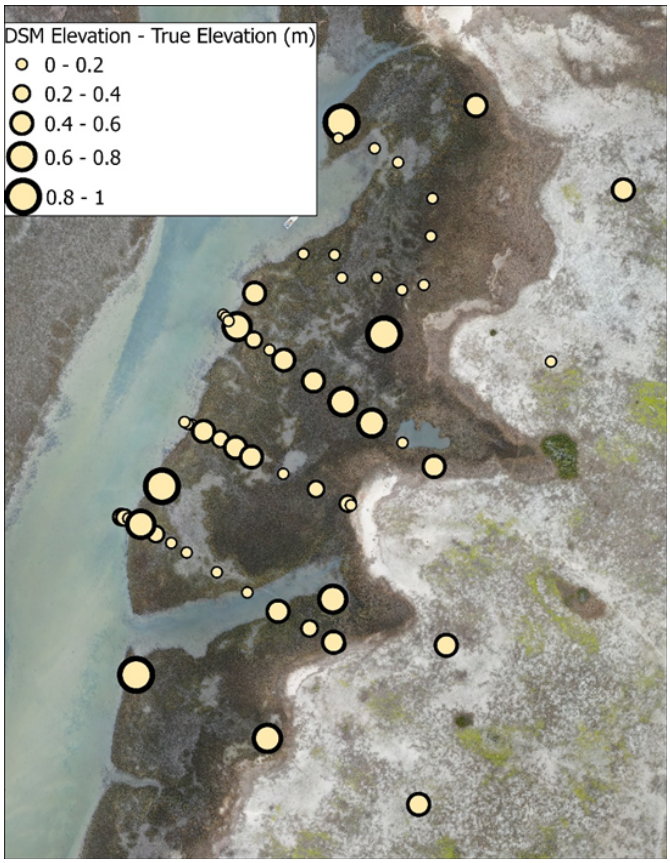

Figure 6. The magnitude of difference between modeled and measured ground truth elevations varies with vegetative density. Larger differences occur in areas of dense vegetation than in areas where ground is visible from the air.

3.4 Point Cloud Filtering

The density of points generated from SfM processing varies with sensor resolution and flight altitude. Metashape-generated dense point clouds from 50 m flights with the Mavic Hasselblad 20 MP RGB sensor averaged 2100 points/m2 while those from the same altitude with the Micasense Altum averaged 500 points/m2. In vegetated areas, the majority of these points will fall somewhere within the vegetative canopy; relatively few will represent the true ground surface. A DTM is created by filtering the SfM-generated point cloud to remove points that don't represent the true ground surface (eg. vegetation, buildings, etc.) and then interpolating across the gaps that are created by filtering (Figure 7). Both Pix4D and Metashape have built-in functions for the generation of DTMs (note that Pix4D refers to this filtered model as a DTM, while Metashape refers to it as a DEM.

In Metashape, point cloud filtration is accomplished with the "classify ground points" tool. The process involves application of a grid with user-defined spacing to the point cloud. The lowest point within each grid cell is selected and categorized as "ground". All points that are greater than a user-defined distance from that low point are filtered out; all remaining points are considered to represent the true ground surface and are incorporated into the DEM. The filtering process can be optimized for any site by altering the max angle, max distance, and cell size parameters within the tool. The ideal settings used for point cloud filtration require trial and error and will vary with differences in topography and vegetation so it is important to adjust each accordingly to optimize the separation of ground and non-ground points. At both of the NERR sites investigated here, a grid size of 2 m, max distance of 0.05 m, and 1° angle resulted in the greatest accuracy for bare earth models.

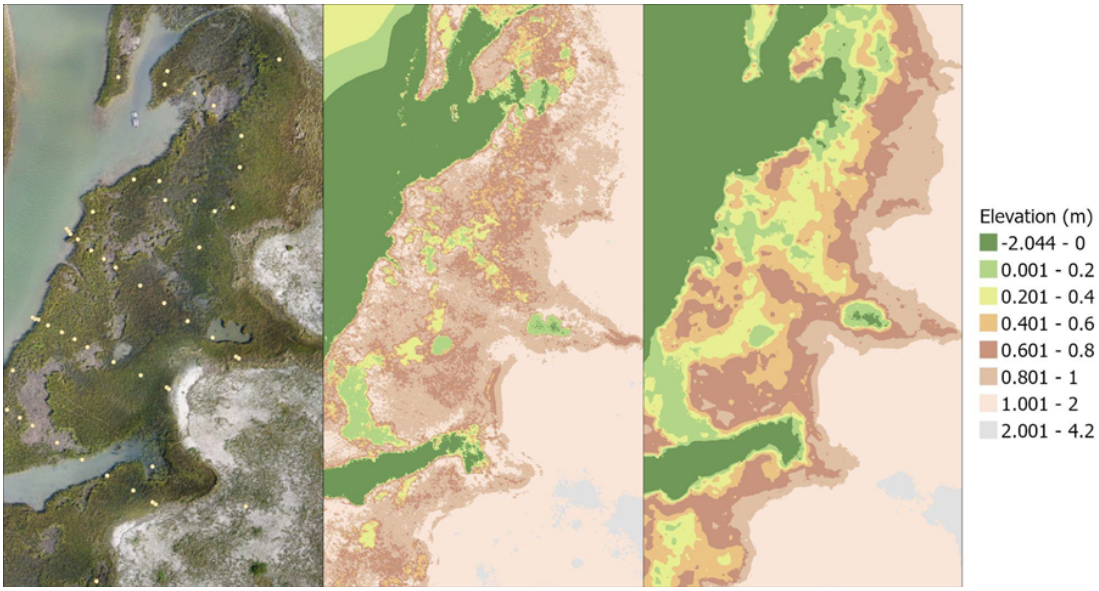

Figure 7. Left: 50 m orthomosaic collected at NCNERR in February 2021. Yellow circles indicate locations of vegetation monitoring plots. Middle: Structure from Motion (SfM)-generated digital surface model (DSM). Right: Bare earth surface model created by point cloud filtration and interpolation in Metashape.

The Pix4D process does not allow for user input, rather the software relies on a proprietary machine learning algorithm using geometry and point color to determine point classification and generate the bare earth model. This is largely successful in many environments, but we note that it struggles in wetland environments. In both software packages, bare earth models exhibited substantially increased agreement with measured ground truth point elevations relative to unfiltered DSMs.

The RMSEz of Metashape computed vs. true elevations of ground truth points decreased by an average of 15 and 21 cm at NIWB and NCNERR respectively across both seasons and all altitudes as a result of point cloud filtration. The RMSEz for PIX4D generated DTM's decreased relative to that of DSMs by 15 and 11 cm at NIWB and NCNERR respectively. Comparison of modeled elevations in the original (DSM) and filtered (DTM) surface models with measured elevations at NCNERR illustrates the impact of point cloud filtration (Figure 8).

To further assess the vertical accuracy of photogrammetrically computed DTMs, these data were compared to that of the most recent bare earth lidar models available through NOAA's data access viewer (https://coast.noaa.gov/dataviewer/#/). The lidar-DTM used for NIWB was collected between December 2016 and March of 2017 and provided by the SC Department of Natural Resources; the lidar DTM used for NCNERR was collected and provided by the US Army Corps of Engineers Joint Airborne Lidar Bathymetry Technical Center of Expertise in September of 2018. To assess vertical accuracy, measured elevation at ground truth points was compared to lidar-generated bare earth models in ArcPro using the approach previously described for SfM-generated surface models (Section 3.3). **SfM-generated DTMs were of comparable accuracy to that of lidar-generated bare earth models** (Figure 9).

3.5 Impacts of Altitude and Season on Model Accuracy

The fidelity with which SfM-constructed models represent the true ground surface is strongly influenced by the presence of vegetation. A dense vegetative canopy obscures the sensor from "seeing" the surface and therefore decreases the possibility of modeling it accurately. Because higher resolution imagery is able to capture greater spatial detail, we postulated that point clouds from lower altitude flights would contain more points that penetrate the vegetative canopy to represent the true ground surface, leading to higher accuracy surface models. We further hypothesized that time of year would influence the accuracy of ground surface models by allowing for a better "look" at the ground surface during winter months when much of the standing above ground biomass has died back.

To evaluate the influence of flight altitude and season on the projection accuracy of image-based products in wetland habitats, we conducted consecutive flights at both NERR sites at altitudes of 25, 50, and 120 m. Imagery was collected in September 2020 and again in February 2021 for a total of six flights per site. In both seasons, the same ground truth points, flight paths, platforms, and sensors were used at each site. In all cases, GCP density was greater than or equal to 0.9 GCP per hectare. The ground sampling distances of the resulting imagery products varied by sensor and altitude (Table 1) and ranged from 6 mm to 5.6 cm. Projection errors were ≤ 7 cm for all data sets and did not vary consistently with GSD.

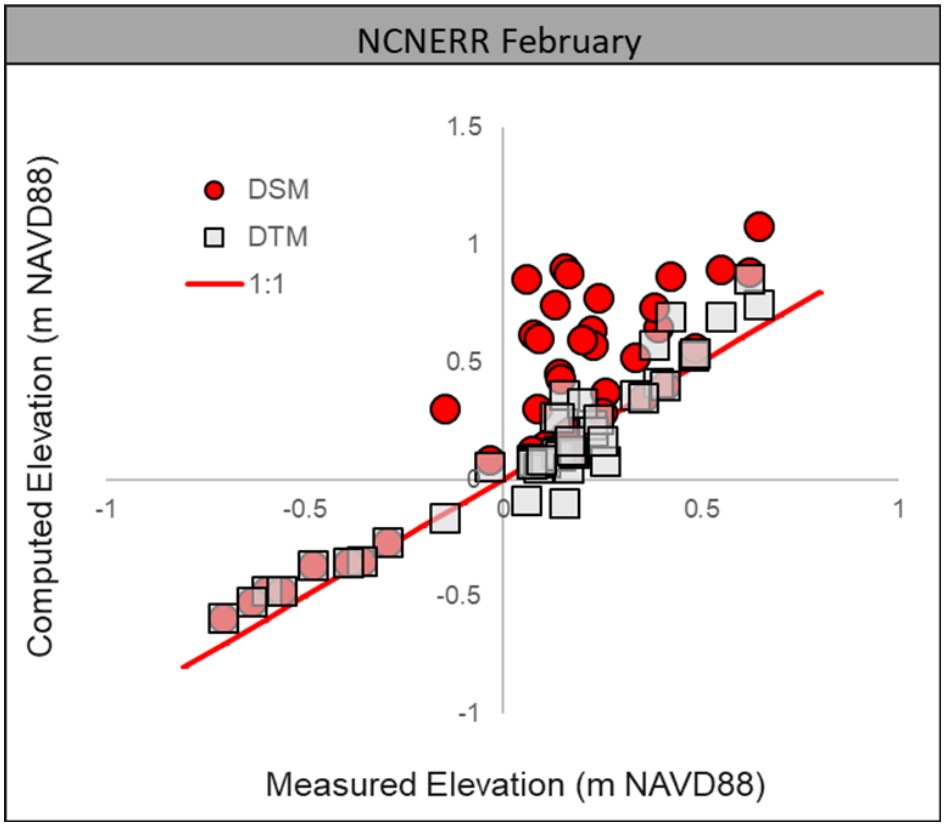

Figure 8. Computed vs measured elevation at ground truth points in digital surface model (DSM, circles) and digital terrain model (DTM, squares) from NCNERR February 2021 imagery illustrates the value of point cloud filtering routines for representing true ground surface elevations. Note these are the same points shown in the figure 7 above. Elevations less than -0.2 m NAVD88 represent unvegetated mudflats; point cloud filtering had no detectable effect on these points. Analysis done using Metashape.

At both sites, the influence of GSD on model accuracy was further assessed by comparison of modeled vs measured elevations at ground truth points. The ground truth points used include locations where ground-based data collections (e.g. long-term vegetation monitoring, biomass harvesting, etc.) occurred in conjunction with the collection of positional data. A total of 48 ground truth points were collected at NCNERR; 68 were collected at NIWB.

Results of these analyses demonstrate the influence of both season and altitude on model accuracy (Figure 10). In all cases, model error was lower for imagery collected at 50 m than 120 m. The magnitude of the difference varied by site and season. At NCNERR, February imagery produced consistently lower error DTMs than September imagery. At NIWB, there was not a consistent relationship between season and accuracy. It is unclear whether this is due to sensor differences, less desirable lighting conditions (February NIWB flights were conducted early in the morning), or true site differences (i.e. less vegetative die-back). With only one exception (50 m September), accuracies of NIWB models were lower than those created from the same altitude at NCNERR, presumably as a result of lower sensor resolution at NIWB (Table 1). **Collectively these data suggest that the creation of SfM-generated bare earth models of vegetated marsh platforms is optimized by increasing image resolution (decreasing GSD) and may be further enhanced by collecting imagery when vegetative density is lowest.**

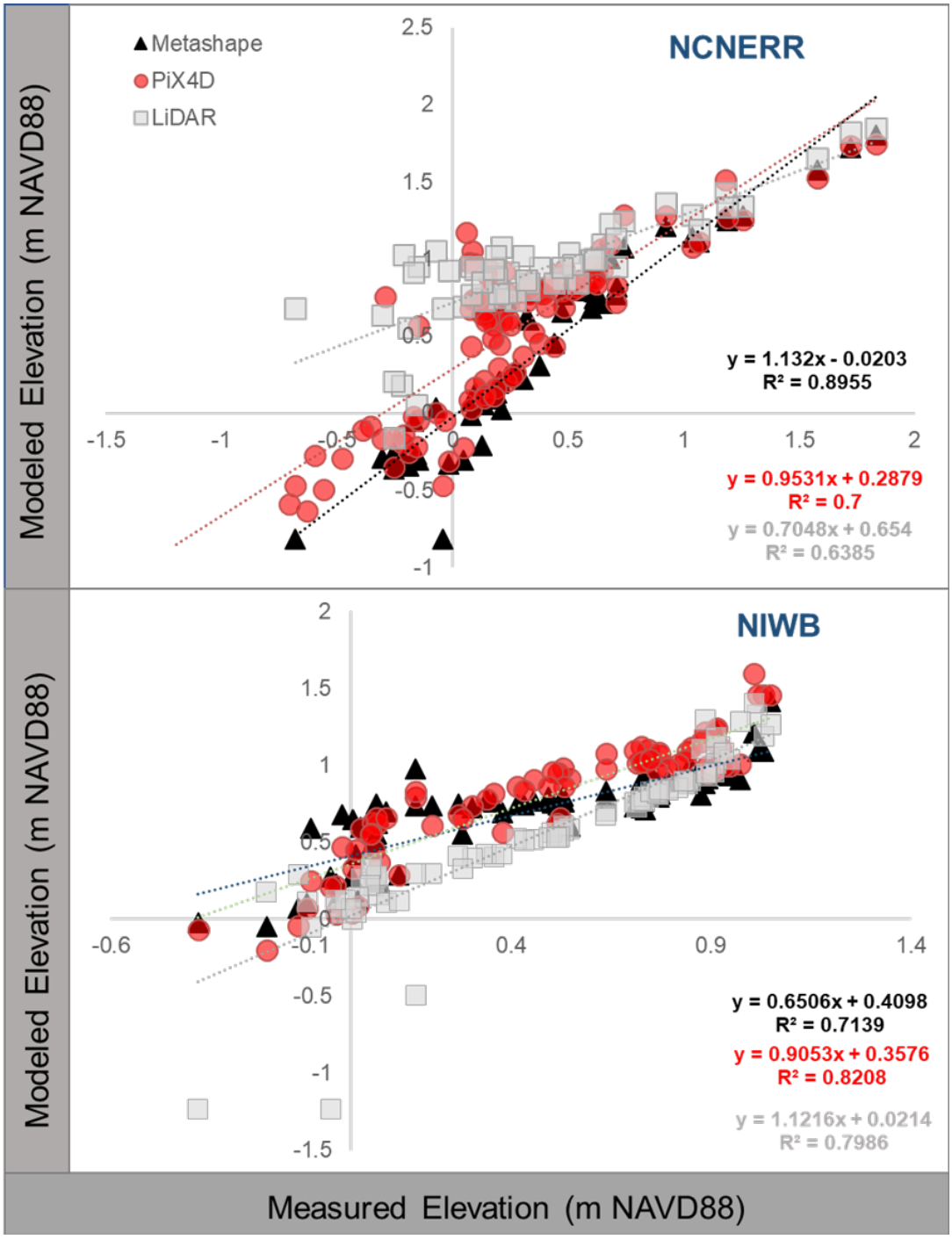

Figure 9. Measured vs structure from motion (SfM)-generated digital terrain model (DTM) and lidar modeled elevations.

4.0 UAS-IMAGE BASED ESTIMATES OF VEGETATIVE CHARACTERISTICS

Most wetland monitoring programs include plot or point based measures of vegetative community composition (i.e. species presence/absence or relative abundance) and/or plant morphometry. Changes in such parameters can be indicative of fundamental shifts in marsh function. Due to the limited spatial coverage associated with point/plot-based sampling, the ability to quantify these same parameters from imagery would greatly increase the power to detect change. The marsh monitoring protocols employed by NERRS (Moore, 2009) involvedocumentation of vegetative characteristics including percent cover by species, stem height/average canopy height, and standing live biomass at fixed 1 m x 1 m monitoring plots. This section describes our efforts to quantify each of these parameters from imagery collected at 50 m altitudes at both sites using field measured values for validation.

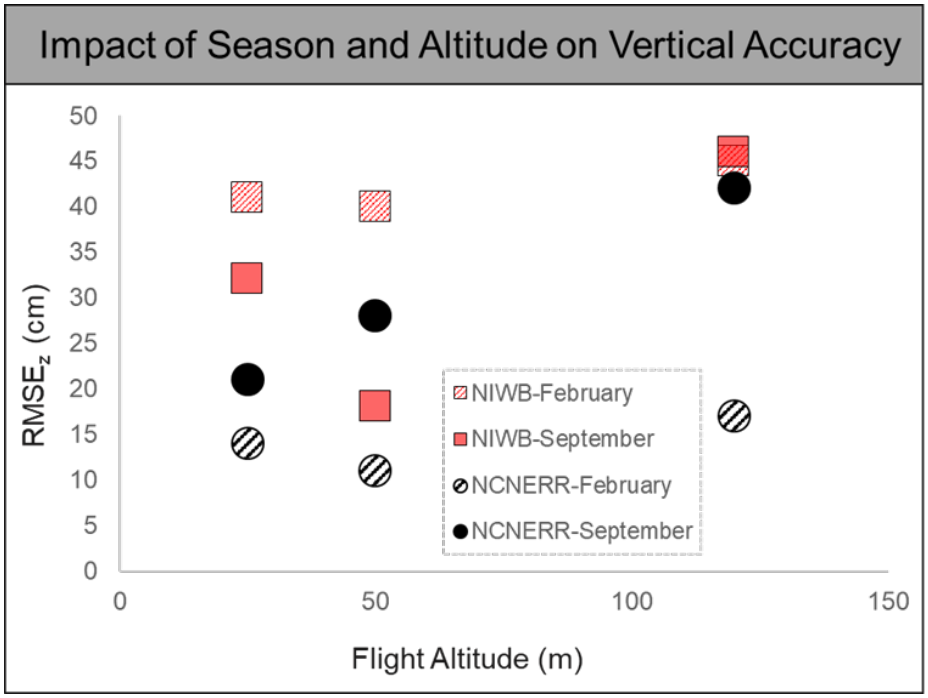

Figure 10. Vertical accuracy of SfM-generated DTMs by site and season and altitude.

Table 1. Projection Error as a function of flight altitude and sensor. Only September 2020 data shown for simplicity of presentation, projection accuracy did not vary between seasons.

Site	Sensor	Altitude (m)	GSD (cm)	X error (RMSE cm)	Y error (RMSE cm)	Z error (RMSE cm)
NIWB	Altum	25	1.2	1.5	1.0	0.2
NIWB	Altum	50	2.3	1.0	0.7	0.9
NIWB	Altum	120	5.6	7.0	4.5	4.6
NCNERR	Hasselblad	25	0.6	2.5	1.6	0.8
NCNERR	Hasselblad	50	1.2	4.0	2.5	0.8
NCNERR	Hasselblad	120	2.8	2.5	2.7	1.9

4.1 Vegetative Percent Cover

Percent cover is typically characterized in the field by either visual observation (ocular estimates) or the point intercept method (Roman et al., 2001). Ocular estimates are quick to perform but highly subjective and can vary from person to person and year to year. To enhance repeatability of the ocular method, coverage is often documented with respect to predefined broad coverage categories (Wikum and Shanholtzer 1978, Peet et al.,1998). The point intercept method is less subjective, but significantly more time consuming to apply.

At NIWB, percent cover was determined using ocular estimates with 5% coverage categories (i.e. 0-5%, 5-10%, etc.). At NCNERR, percent cover was estimated via the point-intercept method. Briefly, a thin rod was lowered perpendicular to the substrate at 50 equally spaced nodes within a 1 m2 quadrat. Plants intercepting the rod at each node were recorded and the total number of occurrences within each quadrat were summed and multiplied by two for a percent cover estimate (0-100%). At both sites, percent cover data was collected during the same week as image collection.

Our objective was to quantify total percent vegetative cover from imagery, not to discern the individual species that contribute to cover. We used two approaches, both of which involved a Normalized Difference Vegetation Index (NDVI)

raster computed from the UAS imagery. NDVI, among the most commonly used spectral indices for classifying and characterizing vegetation, identifies vegetated surfaces by measuring the difference in reflectance between near infrared light (which vegetation reflects) and red light (which vegetation absorbs) (Huang et al., 2021). NDVI was calculated from the Red (R) and NIR bands as (NIR-R/NIR + R) using the band arithmetic tool in ArcGIS Pro. For comparison of NDVI to field-based percent cover estimates, field sampling plots were digitized in ArcGIS by generating a 1 m x 1 m square centered on each GNSS-recorded plot location and the Zonal Statistics tool was used to extract NDVI values of all pixels that fell within the digitized plot (Figure 11). NDVI rasters were generated from images collected at 50 m in September at both NERR sites.

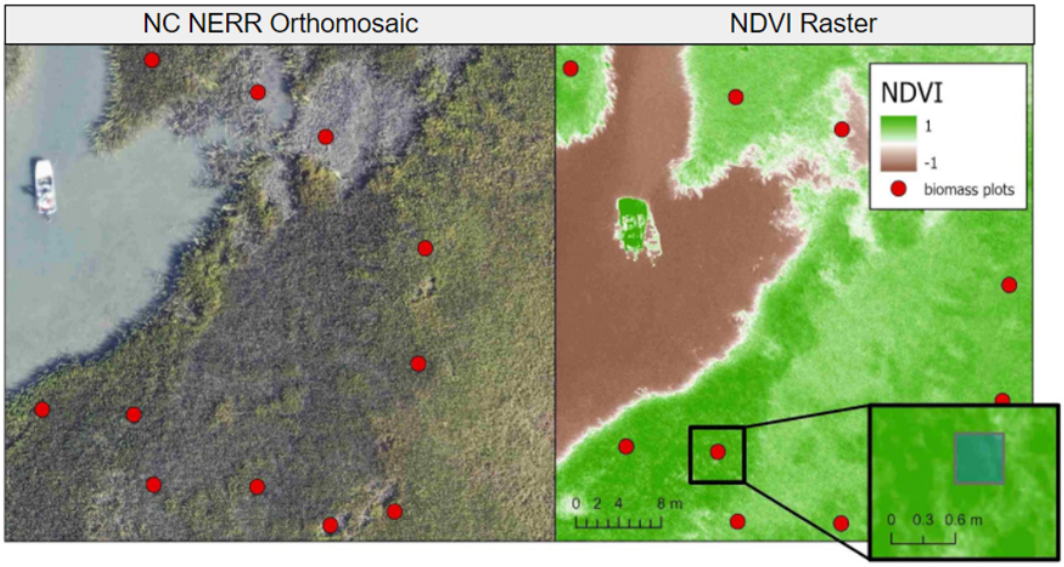

Figure 11. Calculation of NDVI value for each vegetation monitoring plot was accomplished by identifying the plot center in ArcGIS from field collected positional data, then extracting the NDVI values for all pixels that fell within the area of the 1 m x 1 m sample plot.

4.1.1 Thresholding

The first approach used to estimate vegetative percent cover from imagery is referred to here as "thresholding". Thresholding involves the identification of a threshold NDVI value for distinguishing between vegetated and non-vegetated pixels. This was accomplished through visual identification of 30 points that represented vegetation and 30 more that represented bare ground in the orthoimagery from each site. The NDVI value at each point was recorded and then used to determine a threshold value for each site using the following equation:

Threshold = [mean vegetation NDVI - maximum bare ground NDVI]/2.

The threshold value was used to classify all pixels in a plot as either vegetated or unvegetated. Then percent cover was then calculated within each plot as:

Percent Cover = (vegetated pixels/total pixels)*100.

Comparison of computed values of percent cover to field-measured values at fixed monitoring locations indicated a weak correlation between the two (Figure 12).

In general, this approach resulted in overestimation of the amount of vegetation present in a given plot, particularly at NIWB, where computed percent cover values approached 100% in most plots, even those with field measured values as low as 20%.

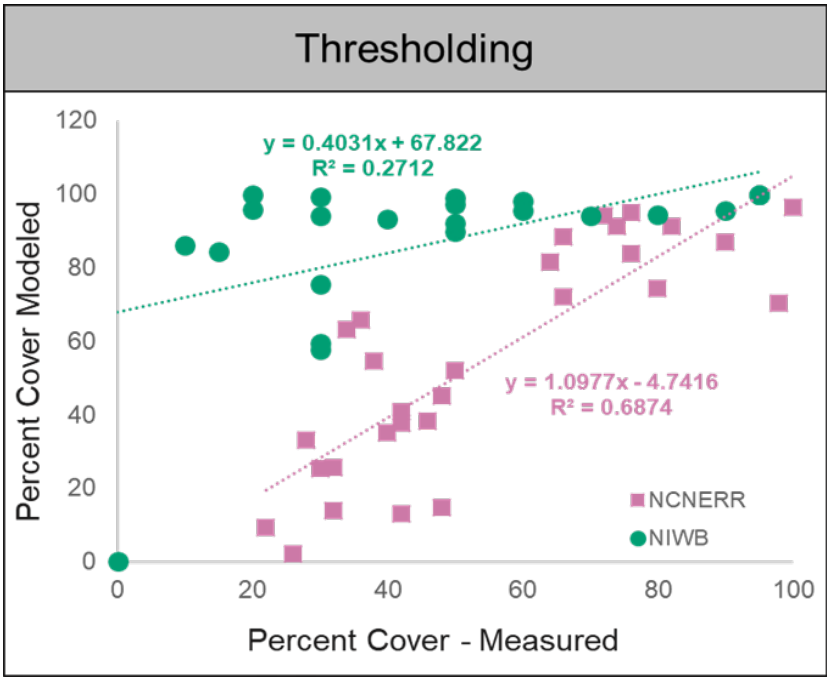

Figure 12. Computed (via thresholding approach) vs field-measured percent cover based on analysis of February and September data sets at both sites.

4.1.2 Averaging

The second approach involved calculating the average NDVI value of all pixels within the area of each monitoring plot and comparing this directly to ground-based cover estimates (Figure 13). This approach relies on the assumption that plots with denser stands of vegetation will have higher average NDVI returns. Due to temporal differences in NDVI signature, this approach requires calibration with ground-based data during every image collection effort but does not require determination of a threshold for vegetation. There was a weak positive correlation between plot averaged NDVI and percent cover at both sites (Figure 13). However, the significant amount of scatter makes it challenging to apply this relationship for predictive purposes with confidence.

Comparison of field-based estimates of percent cover to imagery-computed estimates at the scale of the individual plot are likely impacted by plant morphology and methodology of ground-based assessments, among other factors. In stands where the vegetation is relatively erect (e.g. in an *S. alterniflora* marsh with stem heights < 50 cm), an imagery-computed estimate based on the number of vegetated and unvegetated pixels is likely to be closer to ground-based estimates than when stems are too tall to stand erect (e.g. *S. alterniflora* of > 1.5 m). In the latter case, stems tend to be sparse but individual leaves drape outward from the central stem under their own weight, increasing the aerial coverage of each stem. As a result, image-based estimates are likely to overestimate cover relative to ground based estimates at sites with tall stem heights. **The image-based approaches used here for estimation of percent cover have limited utility for replicating ground-based estimates.** It should be noted that ground-based percent cover estimates (particularly ocular estimates) are highly subjective and thus may not be the appropriate standard against which to assess the accuracy of image-based approaches. Advancements in this area will require consideration of both ground and image-based methods.

4.2. Stem Height

To estimate stem height from imagery data sets we utilized a canopy height model (CHM) approach. The CHM method involves calculating the distance between the ground surface and the vegetative canopy surface by subtraction of the bare earth model (DTM) from the canopy surface model (referred to here as the DSM). To accomplish this, the DTM and DSM for each site were imported into ArcPro and the snap raster tool was used to ensure alignment of raster cells. Average and maximum raster values were extracted from within the digitized area of each sampling plot using the zonal statistics tool and canopy height was estimated using two approaches: mean DSM - mean DTM and max DSM - mean DTM. Stem height ground validation data was collected by measuring the height of the three tallest stems within each plot. Stem heights were measured with plants remaining in their resting positions (i.e. stems were not stretched to their full length for measurement) as the max height that a plant reaches in its resting position is what the camera senses. Comparison of field measured and SfM-computed stem heights demonstrated a weak linear relationship between the two (Figure 14).

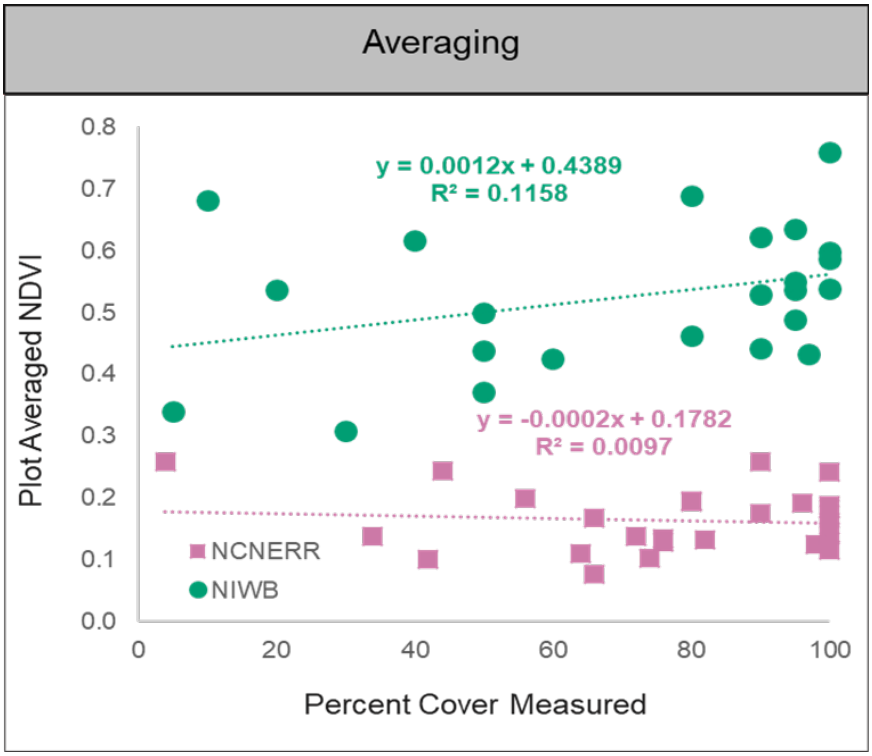

Figure 13. Plot averaged NDVI as a function of field measured percent cover based on September data sets for both sites.

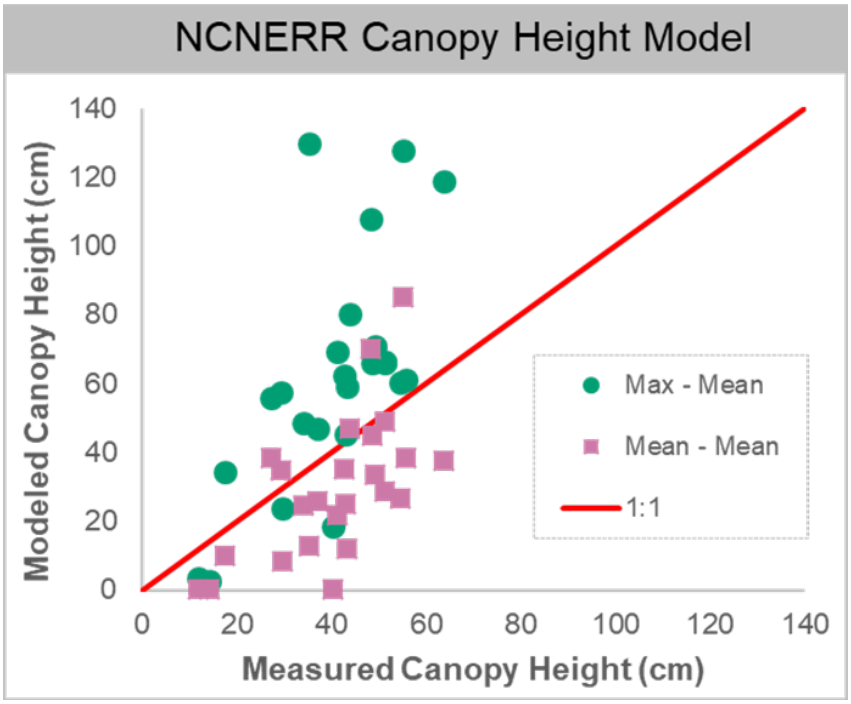

Figure 14. Canopy Height Model based estimates of stem height vs field-measured stem heights.

CHM-based predictions of stem height are influenced by the accuracies of both the DSM and DTM. We have previously demonstrated the average DTM-computed elevations to deviate from true ground elevations by a minimum of 10 cm and for this accuracy to vary spatially with differences in vegetative cover (Section 3 above). **The canopy height model approach, as applied here shows moderate utility in estimation of vegetative canopy height from imagery.** In general, this approach tends to overestimate bare earth elevation and underestimate canopy height elevation. We suggest that it is likely to be most accurate in sparsely vegetated systems (where the ground is visible in imagery between stems) where vegetation is short enough to stand erect.

4.3 Standing Live Biomass

Remote sensing is a critical tool for vegetative biomass estimation and has been widely utilized in coastal wetlands. Remote sensing approaches have traditionally relied upon vegetative indices (combinations of surface reflectance in two or more wavelengths) to provide quantitative and qualitative evaluations of vegetation. The most commonly employed vegetative index for estimation of biomass is NDVI (described above). Previous satellite-based applications have shown that relative differences in NDVI are highly correlated with changes in vegetative biomass over large temporal and spatial scales (Todd et al., 1998, Lumbierres et al., 2017). In most cases, the resolution of satellite-based imagery datasets (10-30 m) is up to two orders of magnitude lower than UAS based imagery (1-5 cm in the current effort).

Our goal was to evaluate the accuracy with which UAS-sensed NDVI predicts on-the-ground estimates of standing biomass made via destructive harvesting. Biomass sampling plots (25 cm x 25 cm) were established in monospecific S. alterniflora at both NERR sites in September of 2020. Standing vegetation was harvested by clipping at the sediment surface. All harvested biomass was washed to remove attached sediments, then dried (60 C for 72 hours) and weighed to the nearest 0.1 g. The center of each sampling plot was identified with RTK-GNSS and this positional information was used to digitize the plots in ArcPro for identification in NDVI rasters created from 50 m altitude flights. The zonal statistics tool was used to extract the mean raster value from within the area of each sampling plot and a simple linear regression between measured biomass and mean NDVI was used to investigate the relationship between the two (Figure 15). Biomass data were square root transformed to satisfy normality requirements.

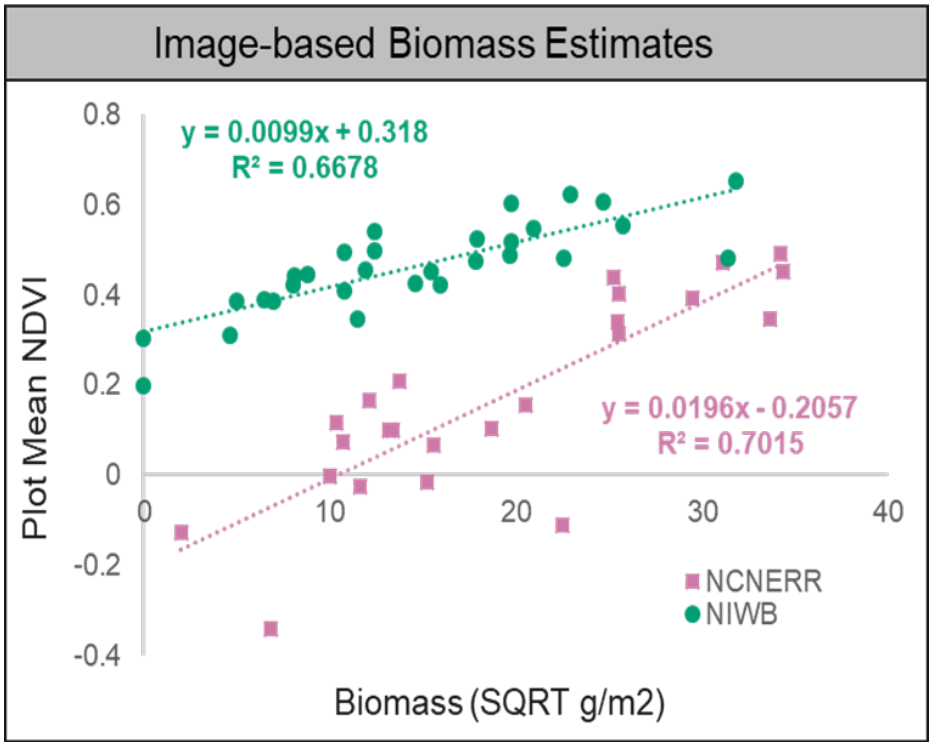

Figure 15. Dry weight of standing live biomass vs mean NDVI signature in monospecific S. alterniflora *plots.*

The regression between measured biomass and mean NDVI revealed a significant relationship between the two, suggesting that **UAS-measured NDVI is effective for predicting live biomass at the scale of the individual monitoring plot.** These data are all for monospecific S. alterniflora stands. Further work is required to determine how well NDVI predicts biomass for plots with mixed species assemblages.

Reflectance is influenced by the concentration of light-absorbing pigments in plant tissue which vary seasonally, with changing environmental conditions, and among different species. As a result, it is not clear how consistent these relationships are over time and space. Comparison between the two sites demonstrated that for a given plot biomass, the mean NDVI value was consistently lower at NCNERR than at NIWB (Figure 16). To investigate whether this was the result of differences between the two sensors used, or true differences between sites, an additional series of flights were conducted in May of 2021 at NCNERR when both platform-sensor combinations were flown sequentially over the same

area. Comparison of plot-averaged NDVI values from the same fixed sampling plots indicates a difference by sensor with the Sentera (NCNERR) consistently reporting lower NDVI values than the Micasense Altum (NIWB) (Figure 16).

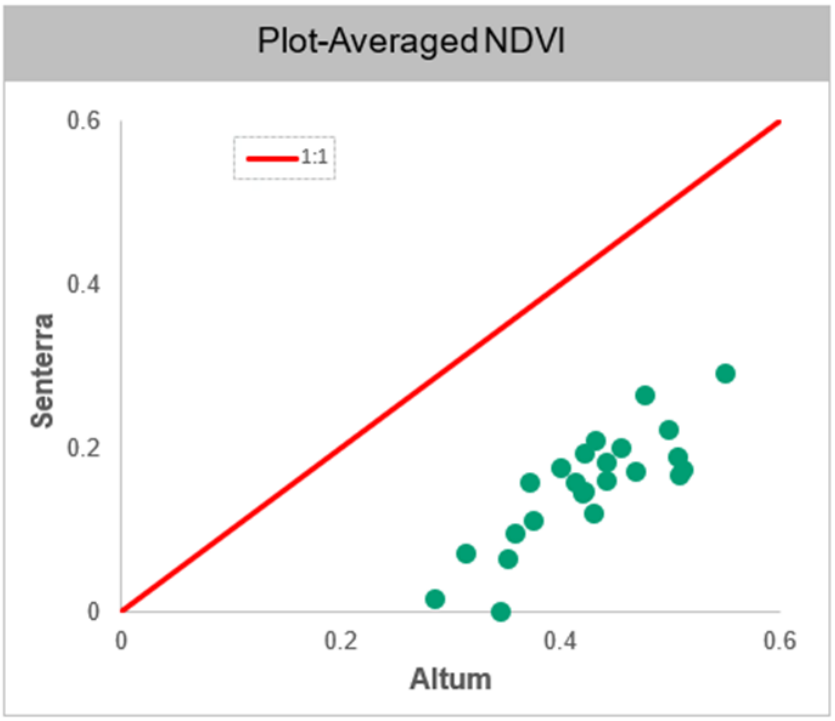

Figure 16. Comparison of data from sequential flights reveals sensor-specific differences in NDVI value.

Sensor to sensor variations in NDVI are presumably the result of differences in the specific band widths detected by different sensors. The red and NIR ranges detected by the Senterra are 615 to 685 nm and 830 to 850 nm respectively, while those detected by the Altum are 660 to 676 nm and 814 to 870 nm. **Subtle differences among sensors make it imperative to cross-calibrate results when comparing data sets that were not collected with the same sensor (eg. when sensors are changed/upgraded during the course of a time series data collection).**

It is important to note when using NDVI to characterize emergent vegetation, other chlorophyll containing organisms can make a significant contribution to measured NDVI. At Swan Island, where a dense periphyton mat colonized large regions of the study area, NDVI signatures associated with the periphyton overlapped with those of the *S. alterniflora* (Figure 17). **Interpretation of NDVI signatures requires in-depth knowledge of the site.** In this example, a DSM can be useful in distinguishing between the two due to the differences in canopy height elevation between periphyton and emergent vegetation.

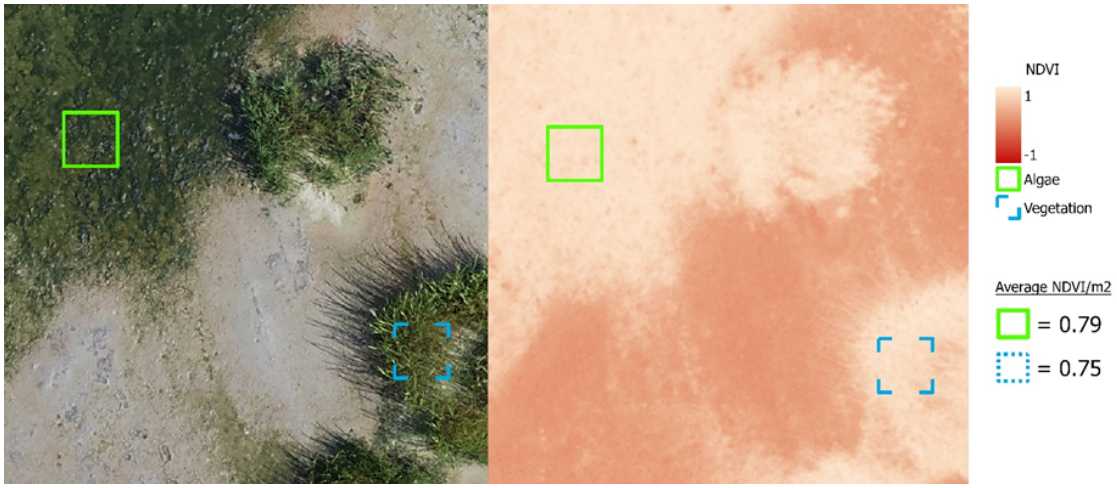

Figure 17. Overlap in NDVI values between benthic periphyton and S. alterniflora *complicates imagery-based quantification of vegetative biomass. Left panel = RGB imagery, Right panel = NDVI raster.*

5.0 HABITAT CLASSIFICATION

Many previous wetland habitat classification efforts have used satellite or aerial imagery to identify wetlands within the wider landscape. The high resolution of UAS imagery makes possible the detection of individual species or communities within a given wetland complex and by extension, changes in the aerial cover of each over time. We conducted supervised object- based image analysis using the Classification Wizard in the ArcGIS Pro Image Analyst extension to generate classified habitat rasters for each of the sites and to evaluate the factors that influence their accuracy. Previous efforts have demonstrated superior performance of object-based, compared to pixel-based classification methods in wetlands, which tend to have limited spectral variability among cover types (Dronova, 2015). Object-based classification utilizes differences in both spectral and spatial properties within an image to group pixels into homogeneous segments. These segments are subsequently classified into cover types based on a user-created training sample dataset. The training data set consists of defined areas within the image that represent the different habitat types of interest. Generation of training datasets requires extensive knowledge of the site and/or ground validation of the vegetative communities to be classified. In the ArcGIS Classification Wizard, the user can vary the degree to which the segmentation process is influenced by spectral vs spatial detail. This tool also provides the option to use an ancillary raster dataset, in addition to RGB imagery, to inform the segmentation process. While there are multiple software options available that allow for greater user control of the classification process and the use of multiple ancillary data sets (e.g. eCognition, ENVI), the goal of this effort is to evaluate the use of products that most wetland scientists and managers will have access to and experience with, thus we limit this effort to ArcGIS. We conducted a sensitivity analysis to investigate the influence of image resolution and incorporation of ancillary data sets on the accuracy of habitat classification maps and to investigate the extent to which species assemblages can be differentiated with this approach.

5.1 Image Resolution

The <10 cm resolution that is common in UAS imagery allows for unprecedented ability to differentiate individual stems of vegetation. The small pixel size has some drawbacks including increased processing time and unwanted noise/high variability among pixels within each vegetative community type as some pixels will capture ground, shadows, etc. in addition to plant tissue. Larger pixel sizes automatically smooth some of the variability within each habitat type but result in decreased ability to discriminate among small patches of unique habitat (Wulder et al., 2004). To evaluate the extent to which the resolution of UAS imagery influences classification accuracy in tidal wetland habitats, classification maps were created using RGB orthomosaics (collected from 50 m altitude) at original resolution which ranged from 1-3 cm/pixel depending on the sensor, and on orthomosaics resampled in ArcGIS to resolutions of 10, 30, 50, 70, and 100 cm/pixel. Training samples were created with guidance from field staff at each location. The same training samples and segmentation parameters (20 spectral detail, 12 spatial detail, 200 minimum segment size) were used for all iterations.

In a perfect world, accuracy of a habitat classification would be verified with ground-based observations. Often, this approach will not be feasible due to the sheer size and/or accessibility of a given site. To evaluate classification accuracy

without boots on the ground, we generated 100 random points for each site using the "Create Random Points" tool in ArcGIS. The 100 points were overlaid on the orthoimagery from each site and classified visually by a field researcher with extensive experience at each site (Figure 18, top). Agreement between modeled and user-defined habitat classifications at each point was assessed through a confusion matrix (breakdown of the number of correct and incorrect predictions by habitat class) based on the assumption that the field researcher-defined classifications were correct (Figure 19, bottom). The accuracy of each classification is calculated as the total number of points at which modeled habitat type and user-defined habitat types were in agreement (sum of yellow highlighted cells in figure 18), divided by the total number of points x 100. **Comparison of classification accuracies among images with varying resolutions indicated a loss of accuracy at resolutions of 20 cm/pixel and fewer** (Figure 19). Increased pixel size resulted in the exclusion of several of the rarer habitat classes from the final product as these areas were essentially averaged into the surrounding habitat types.

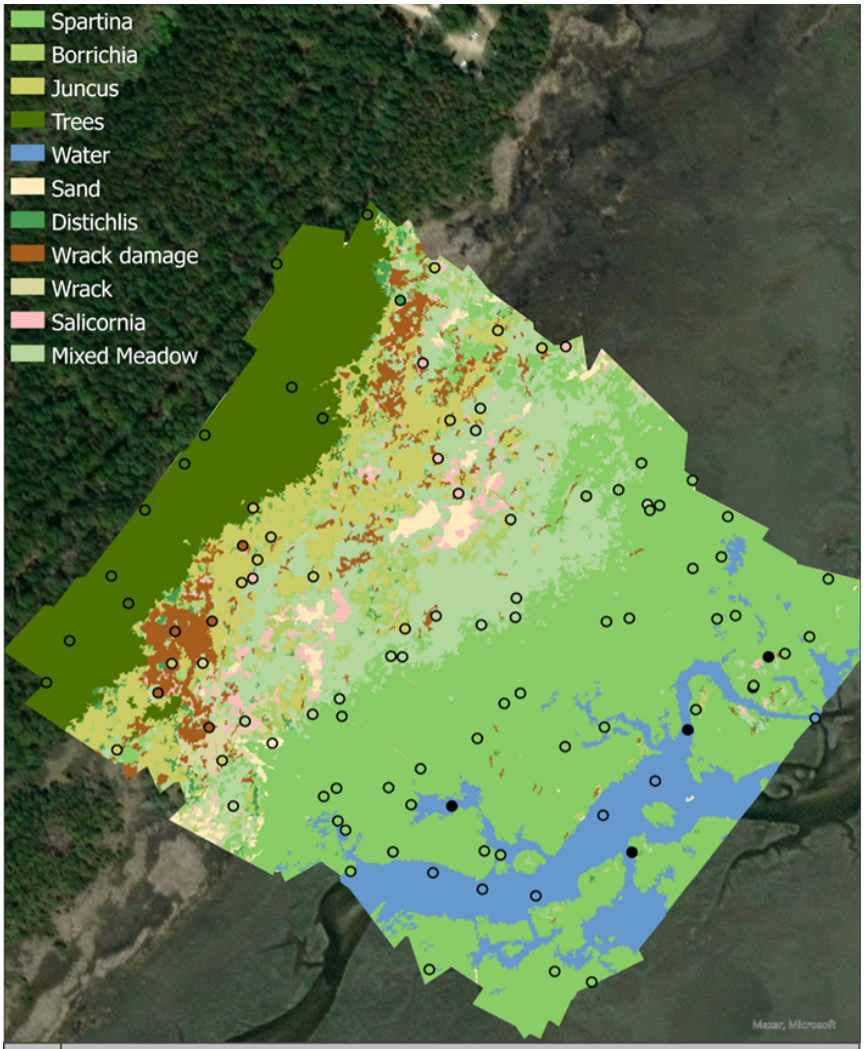

Modeled Habitat Type	Expert-Determined Habitat Type										
	1	2	3	4	5	6	7	8	9	10	11
1	35		1								3
2		0	1							1	1
3			6				1	1	1	1	
4	2		1	11							
5					6						
6						1					
7							0				
8	1		1				1	3		1	1
9									0		
10										0	1
11	1		3					1		2	8

Figure 18. Example assessment of classification accuracy. Top: classified habitat raster created using supervised object-based image analysis with the Classification Wizard in the ArcGIS Pro Image Analyst. Raster indicates modeled habitat type; circle fill color indicates expert determined habitat type. Bottom: confusion matrix evaluates agreement among measures and modeled values (yellow boxes). Model accuracy is calculated as the sum of yellow boxes divided by the total number of points evaluated. Numbers 1-11 (bottom panel) correspond to the order in which habitat types are listed in the legend (top panel).

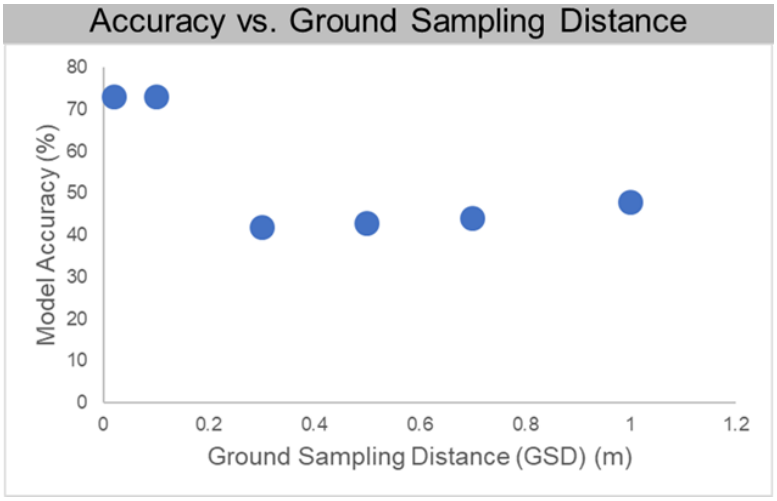

Figure 19. Computed accuracy of habitat classifications decreased substantially with decreased image resolution

5.2 Ancillary Data

Wetlands have limited variability in spatial and spectral detail among vegetation types and this lack of variability presents significant challenges to classification. Habitat classification efforts can be further refined through the use of secondary raster datasets that accentuate differences among the target habitat classes. To investigate the utility of ancillary datasets, we re-classified the 10 cm orthomosaics from each site first using a DSM, and then a second, independent classification was conducted using an NDVI raster as the ancillary data set (Figure 20). The same training samples and classification parameter settings were used for all model runs. The results illustrate the value of additional datasets for optimizing habitat classification. When no ancillary data was included, the classifier struggled to differentiate among vegetation types (and in some areas between vegetation and standing water) based on RGB imagery alone. As a result, large portions of the low marsh (near the tidal creek in the lower right corner of the image) were classified as trees. The use of an NDVI layer significantly improved the ability to distinguish among water and vegetation/bare sediments but did not have a significant impact on the model's ability to distinguish trees from low marsh vegetation. Incorporation of a DSM (in this case representing canopy height) was effective for distinguishing among vegetation types of different heights as well as between vegetation and bare earth and resulted in a significantly improved classification. **The addition of an ancillary data set can substantially improve wetland habitat classifications.** Any raster data can be used as an ancillary dataset in the ArcGIS classification workflow. The best choice will vary by site with differences in physical structure and spectral properties.

Image classification involves grouping individual pixels into categories (termed "segments" in ArcPro) based on similarities in their spectral signatures. Consequently, larger spectral differences among the target habitat classes lead to more accurate classifications. In most cases, it will not be possible to discriminate between individual species with RGB imagery, as the signatures of many wetland plants overlap. There is some trial and error involved with determining how many classes can be reliably discriminated in any image set and overall accuracy of the classification may be improved by condensing species into spectrally similar groups where possible. Further, it may be beneficial to time image collection for seasons when the species/communities of interest are most distinct. We have had success (overall accuracies ranging from 75-85%) using RGB imagery and a DSM across a range of sites in the mid-Atlantic and Southeastern US distinguishing among the categories: low marsh (*S. alterniflora*), high-mixed marsh (*S. patens, Distichlis spicata*, *Salicornia sp*.) *Juncus romerianus*, and woody shrubs (*Baccharis halimifolia, Iva frutescens, Phragmites sp.*).

Wetland habitat classification from UAS imagery (much like SfM photogrammetry) is a modeling exercise in which no two solutions are exactly the same. Each site requires trial and error and what works best in one season may not be the best solution in another; the user needs to be comfortable with some degree of uncertainty. Even so, **it is possible for an entry level user to map functional habitat types within a given wetland with a high degree of confidence based on RGB imagery alone.**

6.0 FUTURE RESEARCH NEEDS

UAS are a valuable addition to wetland monitoring efforts, and will dramatically increase the ability to detect change at the temporal and spatial scales that are important to wetland scientists and managers. The data presented here demonstrate that with attention to detail, it is possible to create high quality 2- and 3-dimensional data sets with a relatively inexpensive platform, basic RGB sensor, and minimal experience. Despite the demonstrated value of UAS for augmenting on-the-ground monitoring efforts, a number of important challenges remain to be addressed by future research efforts.

The work presented here indicates that NDVI is significantly correlated with standing biomass of *S. alterniflora* at the scale of individual monitoring plots. It is not clear how effectively NDVI can predict plant biomass in tidal systems with mixed species assemblages, nor how robust such predictions would be to minor changes in relative abundance of the various species present. **Further research defining the relationships between NDVI and live biomass in mixed species assemblages is needed to facilitate image-based quantification of live biomass at the whole marsh scale.**

DSMs produced from UAS imagery through photogrammetry are comparable in accuracy to those produced from lidar collected from crewed-airplane surveys. While there are significant trade-offs between the two data collection methods (e.g. the greater spatial coverage of crewed flights but lesser cost of UAS flights) they share the common limitation of decreased accuracy of bare earth models over vegetated areas. In recent years, the availability of UAS-based lidar units has expanded rapidly and costs of such units have decreased, making UAS-based lidar collection a viable option for many researchers. Early comparisons of UAS-lidar vs imagery-generated surface models have reached conflicting conclusions about which data type produces higher quality surface models, and seem to indicate that the accuracy of each is strongly determined by point cloud density (Kalacska et al., 2021, Pinton et al., 2021). **Further investigation of the use of UAS lidar both alone, and in combination with photogrammetry is needed to determine the optimal solution for surface model generation.**

Development of a standardized approach for wetland monitoring that considers both ground-based sampling and image collection activities is needed. Although there is currently no widely agreed upon set of guidelines for on the ground wetland monitoring, most monitoring programs include collection of data on species presence and abundance, plant height, and delineation of ecotones. While the targeted metrics are often similar among programs, the methods used can vary widely and some are much more directly comparable with UAS-based approaches than others. For example, measures of canopy height that target the tallest plants in a plot are less valuable for ground-truthing imagery than estimates of average canopy height. Incorporation and advancement of image-based monitoring approaches has the potential to result in increased reproducibility of observations and enhanced ability to detect change at the scale of the whole marsh.

The above recommendations for further research only scratch the surface of what remains to be done to capitalize on the full benefit of UAS platforms for wetland monitoring and detection of changes over time. Continued advances in platforms, sensors and image analysis-software will enhance the value and ease of use of UAS-based imagery and lead to novel applications. Still, even at the current stage of development, this technology is invaluable for monitoring change in coastal wetland habitats.

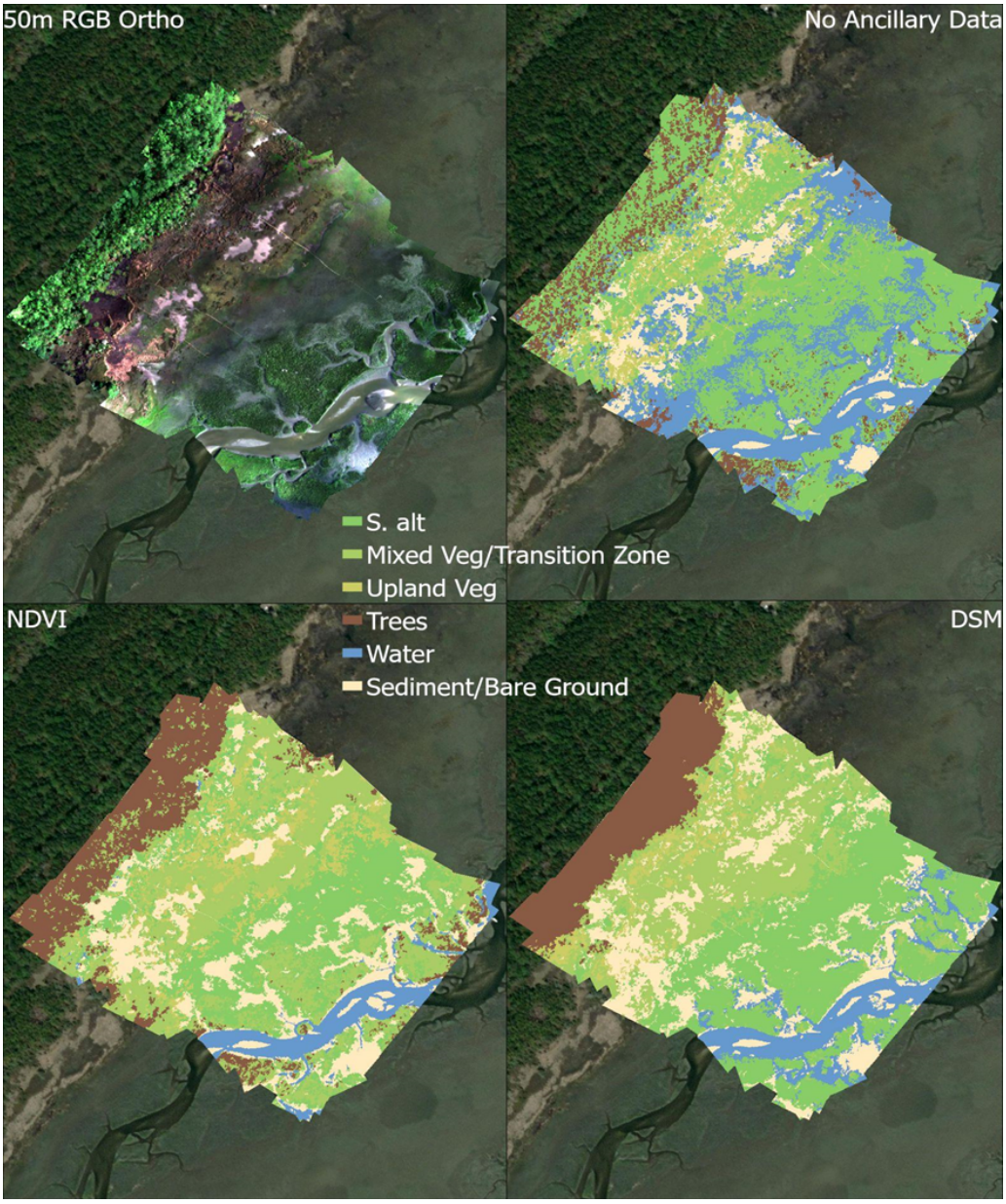

*Figure 20. Habitat classifications can be improved when ancillary datasets are incorporated into the processing. Top Left: Orthomosaic image of NIWB marsh collected at 50 m altitude. Top Right: Supervised habitat classification performed using only RGB imagery (i.e. no ancillary data was used). Bottom Left: Habitat classification performed using NDVI raster as an ancillary dataset. Bottom Right: Habitat classification performed using digital surface model (representing vegetative canopy height) as an ancillary data set.*5). Investigate the potential impact of the landfill on other nearby systems (e.g. Fagalua/Fogoma).

References

Assmann, J.J., J.T. Kerby, A.M. Cunliffe, and I.H. Myers-Smith. 2018. Vegetation monitoring using multispectral sensors – best practices and lessons learned from high latitudes. Journal of Unmanned Vehicle Systems. 7(1): 54-75. https://doi.org/10.1139/juvs-2018-0018

Dobroski, K. 2019. Unoccupied aircraft system applications for salt marsh shorelines: A handbook

Dronova, I. 2015. Object-based image analysis in wetland research: A review. Remote Sensing. 7(5): 6380-6413. https://doi.org/10.3390/rs70506380

Haskins, J., C. Endris, A.S. Thomsen, F. Gerbl, M.C. Fountain, and K. Wasson. 2021. UAV to Inform Restoration: A Case Study From a California Tidal Marsh. Frontiers in Environmental Science. 9: 642906. https://doi.org/10.3389/fenvs.2021.642906

Huang, S., L. Tang, J.P. Hupy, Y. Wang, and G. Shao. 2021. A commentary review on the use of normalized difference vegetation index (NDVI) in the era of popular remote sensing. Journal of Forestry Research. 32: 1-6. https://doi.org/10.1007/s11676-020-01155-1

James, M.R., S. Robson, S. d'Oleire-Oltmanns, and U. Niethammer. 2017. Optimising UAV topographic surveys processed with structure-from-motion: Ground control quality, quantity and bundle adjustment. Geomorphology. 280: 51-66. http://doi.org/10.1016/j.geomorph.2016.11.021

Jeziorska, J. 2019. UAS for Wetland Mapping and Hydrological Modeling. Remote Sensing. 11: 1997. https://doi.org/10.3390/rs11171997

Joyce, S., F. Shand, J. Tighe, S.J. Laurent, R.A. Bryant, and S.B. Harvey. 2018. Road to resilience: a systematic review and meta-analysis of resilience training programmes and interventions. BMJ Open. 8(6). http://doi.org/10.1136/bmjopen-2017-017858

Kalacska, M., G.L. Chmura, O. Lucanus, D. Bérubé, and J.P. Arroyo-Mora. 2017. Structure from motion will revolutionize analyses of tidal wetland landscapes. Remote Sensing of Environment. 199: 14-24. http://doi.org/10.1016/j.rse.2017.06.023

Kalacska, M., J.P. Arroyo-Mora, and O. Lucanus. 2021. Comparing UAS LiDAR and Structure-from-Motion Photogrammetry for Peatland Mapping and Virtual Reality (VR) Visualization. Drones. https://doi.org/10.3390/drones5020036

Lumbierres, M., P.F. Méndez, J. Bustamante, R. Soriguer, and L. Santamaría. 2017. Modeling Biomass Production in Seasonal Wetlands Using MODIS NDVI Land Surface Phenology. Remote Sensing. 9: 392. https://doi.org/10.3390/rs9040392

Moore, K. 2009. NERRS SWMP Bio-Monitoring Protocol Long-term Monitoring of Estuarine Submersed and Emergent Vegetation Communities. National Estuarine Research Reserve System. Technical Report.

Over, J.R., Ritchie, A.C., Kranenburg, C.J., Brown, J.A., Buscombe, D., Noble, T., Sherwood, C.R., Warrick, J.A., and Wernette, P.A.. 2021. Processing coastal imagery with Agisoft Metashape Professional Edition, version 1.6— Structure from motion workflow documentation: U.S. Geological Survey Open-File Report 2021–1039, 46 p. https://doi.org/10.3133/ofr20211039

Peet. R.K., T.R. Wentworth and P.S. White. 1998. A flexible, mutipurpose method for recording vegetation composition and structure. Castanea 63(3): 262-274.

Pell, T., J.Y.Q. Li, and K.E. Joyce. 2022. Demystifying the Differences between Structure-from-Motion Software Packages for Pre-Processing Drone Data. Drones. 6(1): 24. https://doi.org/10.3390/drones6010024

Pinton, D., A. Canestrelli, B. Wilkinson, P. Ifju, and A. Ortega. 2021. Estimating Ground Elevation and Vegetation Characteristics in Coastal Salt Marshes Using UAV-Based LiDAR and Digital Aerial Photogrammetry. Remote Sensing. 13(22): 4506. https://doi.org/10.3390/rs13224506

Roman, C.T., M. James-Pirri, and J.F. Heltshe. 2001. Monitoring Salt Marsh Vegetation: A protocol for the long-term coastal ecosystem monitoring program at cape cod national seashore. U.S. National Park Service.

Saha, A.K., M.K. Arora, E. Csaplovics, and R.P. Gupta. 2005. Land Cover Classification Using IRS LISS III Image and DEM in a Rugged Terrain: A Case Study in Himalayas. Geocarto International. 20(2): 33-40. https://doi.org/10.1080/10106040508542343

Santana, L.S., G.A.E. Sila Ferraz, D.B. Marin, B.D.S. Barbosa, L.M. Dos Santos, P.F.P. Ferraz, L. Conti, S. Camiciottoli, and G. Rossi. 2021. Influence of flight altitude and control point in the georeferencing of images obtained by unmanned aerial vehicles. European Journal of Remote Sensing. 54: 59-71,

Slocum, R.K., W. Wright, C. Parrish, B. Costa, M. Sharr, and T.A. Battista. 2019. Guidelines for Bathymetric Mapping and Orthoimage Generation using sUAS and SfM, An Approach for Conducting Nearshore Coastal Mapping. NOAA Technical Memorandum NOS NCCOS 265. https://doi.org/10.25923/07mx-1f93

Sona, G., L. Pinto, D. Pagliari, D. Passoni, and R. Gini. 2014. Experimental analysis of different software packages for orientation and digital surface modelling from UAV images. Earth Science Informatics. 7: 97-107. https://doi.org/10.1007/s12145-013-0142-2

Swayze, N.C., W.T. Tinkham, J.C. Vogeler, and A.T. Hudak. 2021. Influence of flight parameters on UAS based monitoring of tree height, diameter and density. Remote Sensing of Environment. https://doi.org/10.1016/j.rse.2021.112540

Taylor, J.C., D.W. Johnston, J.T. Ridge, W. Jenkins, A. Wakely, D. Hernandez, S. Robinson, J. McCombs, S. Eastman, and K. Dietz. 2021. Drones in the Coastal Zone: Report From a Regional Workshop for the US Southeast and Caribbean. NOAA NOS NCCOS Technical Memorandum 294. 22 pp. doi:10.25923/g9m4-ts27

Todd, S.W., Hoffer, R.M., Milchunas, D.G., 1998. Biomass estimation on grazed and ungrazed rangelands using spectral indices. International Journal of Remote sensing. 19. 427–438.

Tmušić, G., S. Manfreda, H. Aasen, M.R. James, G. Gonçalves, E. Ben-Dor, A. Brook, M. Polinova, J.J. Arranz, J. Mészáros, R. Zhuang, K. Johansen, Y. Malbeteau, I.P. de Lima, C. Davids, S. Herban, and M.F. McCabe. 2020. Current Practices in UAS-based Environmental Monitoring. Remote Sensing. 12: 1001. https://doi.org/10.3390/rs12061001

Westoby, M.J., J. Brasington, N.F. Glasser, M.J. Hambrey, and J.M. Reynolds. 2012. 'Structure-from-Motion' photogrammetry: A low-cost, effective tool for geoscience applications. Geomorphology. 179: 300-314. https://doi.org/10.1016/j.geomorph.2012.08.021

Wikum, D.A. and G.F. Shanholtzer. 1978. Application of the Braun-Blanquet cover-abundance scale for vegetation analysis in land development studies. Environmental Management. 2: 323-329. https://doi.org/10.1007/BF01866672

Wulder, M.A., R.J. Hall, N.C. Coops, and S.E. Franklin. 2004. High spatial resolution remotely sensed data for ecosystem characterization. BioScience. 54: 511-521. https://doi.org/10.1641/0006-3568(2004)054[0511:HSRRSD]2.0.CO;2

Zimmerman, T., K. Jansen, and J. Miller. 2020. Analysis of UAS Flight Altitude and Ground Control Point Parameters on DEM Accuracy along a Complex, Developed Coastline. Remote Sensing. 12(4): 2305. https://doi.org/10.3390/rs12142305

U.S. Department of Commerce

Gina M. Raimondo, *Secretary*

National Oceanic and Atmospheric Administration

Richard W. Spinrad, *Under Secretary for Oceans and Atmosphere*

National Ocean Service

Nicole LeBoeuf, *Assistant Administrator for Ocean Service and Coastal Zone Management*

The mission of the National Centers for Coastal Ocean Science is to provide managers with scientific information and tools needed to balance society's environmental, social and economic goals. For more information, visit: http://www.coastalscience.noaa.gov/